

Deactivation of Ti-based and γ - Al_2O_3 Catalysts in Liquid-phase Methyl Oleate
Epoxidation Reaction



A Thesis Submitted in Partial Fulfillment of the Requirements
for the Degree of Master of Engineering in Chemical Engineering

Department of Chemical Engineering

FACULTY OF ENGINEERING

Chulalongkorn University

Academic Year 2019

Copyright of Chulalongkorn University

การเสื่อมสภาพบนตัวเร่งปฏิกิริยากลุ่มไทเทเนียมและแกมมาอลูมินาสำหรับปฏิกิริยาอีพอกซิเดชัน
ของเมทิลโอเลิเอตในสถานะของเหลว



วิทยานิพนธ์นี้เป็นส่วนหนึ่งของการศึกษาตามหลักสูตรปริญญาวิศวกรรมศาสตรมหาบัณฑิต
สาขาวิชาวิศวกรรมเคมี ภาควิชาวิศวกรรมเคมี
คณะวิศวกรรมศาสตร์ จุฬาลงกรณ์มหาวิทยาลัย
ปีการศึกษา 2562
ลิขสิทธิ์ของจุฬาลงกรณ์มหาวิทยาลัย

กนกพล ม่วงทอง : การเสื่อมสภาพบนตัวเร่งปฏิกิริยากลุ่มไทเทเนียมและแกมมาอลูมินา สำหรับปฏิกิริยาอีพอกซิเดชันของเมทิลโอเลตในสภาวะของเหลว. (Deactivation of Ti-based and γ -Al₂O₃ Catalysts in Liquid-phase Methyl Oleate Epoxidation Reaction) อ.ที่ปรึกษาหลัก : ศ.ปิยะสาร ประเสริฐธรรม, อ.ที่ปรึกษาร่วม : ศุภฤกษ์ ประเสริฐธรรม

เพื่อจำกัดข้อเสียบางประการของตัวเร่งปฏิกิริยาชนิดวิวิธพันธ์นั้นคือ ความสามารถในการฟื้นฟูสภาพและนำกลับมาใช้ใหม่ที่ต่ำ ดังนั้นการเสื่อมสภาพบนตัวเร่งปฏิกิริยากลุ่มไทเทเนียมและแกมมาอลูมินาสำหรับปฏิกิริยาอีพอกซิเดชันของเมทิลโอเลตในวัฏภาคของเหลวที่อุณหภูมิ 50 องศาเซลเซียสจึงนำมาศึกษา จากผลการทดลองพบว่า การเสื่อมสภาพบนตัวเร่งปฏิกิริยากลุ่มไทเทเนียมและแกมมาอลูมินาเกิดขึ้นได้ 2 แบบ ดังนี้ แบบที่ 1 คือการเกิดตะกอนบนตัวเร่งปฏิกิริยา ซึ่งเป็นการเสื่อมหลักของปฏิกิริยานี้ซึ่งพบว่า มี 3 ชนิด ชนิดที่ 1 ถูกพบใน ไทเทเนียมไดออกไซด์และแกมมาอลูมินา ชนิดที่ 2 ไม่ถูกพบในไทเทโนซิลิเกตและแกมมาอลูมินา ชนิดที่ 3 ถูกพบในแกมมาอลูมินาเท่านั้น จากผลของเทคนิคอินฟราเรดสเปกโตรสโคปีเปิดเผยว่า ตะกอนชนิดที่ 1 เป็นแบบหมู่ฟังก์ชันแอลเคนและแอลกอฮอล์ ตะกอนชนิดที่ 2 เป็นแบบหมู่ฟังก์ชันแอลฟา-เบต้าคีโตนที่ไม่อิ่มตัวและแอลเคน ตะกอนชนิดที่ 3 เป็นแบบหมู่ฟังก์ชันเอสเทอร์และแอลเคน สำหรับการเสื่อมสภาพแบบที่ 2 คือ การสูญเสียส่วนที่ว่องไวต่อการเกิดปฏิกิริยาเนื่องจากการเกิดช่องว่างของโมเลกุลออกซิเจนบนพื้นผิวตัวเร่งและการชะละลายของโลหะเนื่องจากตรวจพบปริมาณไทเทเนียมและอลูมินาในตัวอย่างหลังจากเกิดปฏิกิริยา นอกจากนี้อัตราการเสื่อมสภาพของแกมมาอลูมินามีค่าสูงกว่าตัวเร่งปฏิกิริยาชนิดไทเทเนียมไดออกไซด์และไทเทโนซิลิเกต เพราะ ตะกอนที่เกิดบนแกมมาอลูมินานั้นมีแรงยึดเกาะบนตัวเร่งปฏิกิริยามากกว่าตัวอื่นๆ ด้วยเหตุนี้ตะกอนบนตัวเร่งปฏิกิริยาไทเทเนียมไดออกไซด์และไทเทโนซิลิเกตจะถูกกำจัดออกโดยการเผาด้วยอากาศที่อุณหภูมิ 500 องศาเซลเซียส แต่ไม่ใช่กับแกมมาอลูมินาต้องใช้อุณหภูมิในการเผาถึง 700 องศาเซลเซียส การเกิดช่องว่างของออกซิเจนเป็นสาเหตุที่ทำให้ความสามารถในการฟื้นฟูสภาพและนำกลับมาใช้ใหม่ต่ำลงหลังจากฟื้นฟูสภาพด้วยการเผาแล้ว

สาขาวิชา วิศวกรรมเคมี

ปีการศึกษา 2562

ลายมือชื่อนิสิต

ลายมือชื่อ อ.ที่ปรึกษาหลัก

ลายมือชื่อ อ.ที่ปรึกษาร่วม

6170101021 : MAJOR CHEMICAL ENGINEERING

KEYWORD: P25 TS-1 and γ -Al₂O₃ catalysts; deactivation; regeneration; fouling; oxygen vacancy; leaching; methyl oleate epoxidation

Kanokpon Maungthong : Deactivation of Ti-based and γ -Al₂O₃ Catalysts in Liquid-phase Methyl Oleate Epoxidation Reaction . Advisor: Prof. PIYASAN PRASERTHDAM, Ph.D. Co-advisor: SUPAREAK PRASERTHDAM, Ph.D.

To eliminate some drawback of heterogeneous catalysts as a low stability, the deactivation scheme and surface regeneration of TiO₂ (P25), TS-1 and γ -Al₂O₃ catalysts was investigated on the liquid-phase methyl oleate epoxidation reaction at 50 °C. Based on the results, there are two deactivation effects illustrated on the surface after the reaction: (1) the fouling effects are found the main deactivation on this reaction. There are three types which type 1 is found in P25 and γ -Al₂O₃, type 2 is uncovered in TS-1 and γ -Al₂O₃, and type 3 is appeared in γ -Al₂O₃ only. The FT-IR reveals that are alkane (C-H) and alcohol groups (O-H) as a type 1, α,β -unsaturated ketone (C=O) and alkane groups (C-H) as a type 2, and stretching ester (C=O) and alkane groups (C-H) as a type 3, (2) the loss of active species due to the oxygen vacancy forming after the reaction and the leaching effect. Furthermore, the percentage of lower MO conversion of γ -Al₂O₃ is higher than P25 and TS-1 because the obtained fouling on the γ -Al₂O₃ surface is stronger adsorption than P25 and TS-1. For this reason, the fouling deposits on P25 and TS-1 were eliminated completely at 550 °C, but not for γ -Al₂O₃ (700 °C). The O_v sites provide the defects on the surface which the MO conversion cannot return back to the conversion of fresh catalyst.

Field of Study: Chemical Engineering

Academic Year: 2019

Student's Signature

Advisor's Signature

Co-advisor's Signature

ACKNOWLEDGEMENTS

Foremost I would like to express my deep and sincere gratitude to my advisor, Professor Piyasan Prasertthdam, Ph.D. and my co-advisor, Dr. Supareak Prasertthdam, Ph.D. for giving me the opportunity to do this research and the continuous supporting about the problem from the experiment and thesis writing. Their guidance helped me to solve the doubtfulness and give the new directions. In addition, I would like to thank Dr.Meena Rittiruum, Postdoc. for recommending me the result management. This thesis would not be completely achieved without their advice.

Besides I would like to thank the rest of my thesis committee, Dr. Chalida Klaysom, Ph.D. as the chairman, Professor Suttichai Assabumrungrat, Ph.D. and Assistant Professor Okorn Mekasuwandumrong, Ph.D. as my committee members of the thesis for their encouragement and giving the invariably insightful suggestion to upgrade this research and self-improvement further.

Additionally, this project is supported by “Innovation and technology foresight in catalysis and catalytic reaction engineering for biodiesel, ethanol, and catalyst-related industry for sustainable development (CAT-REC Industrial Project)” and the Global Green Chemical Public Company Limited (GGC) to manage the overall expenses between doing the experiment.

Last but not least, I most gratefully acknowledge my beloved family and friends for encouragement and stimulation until the last period of this research. As, this thesis would unlikely be successful without their supports.

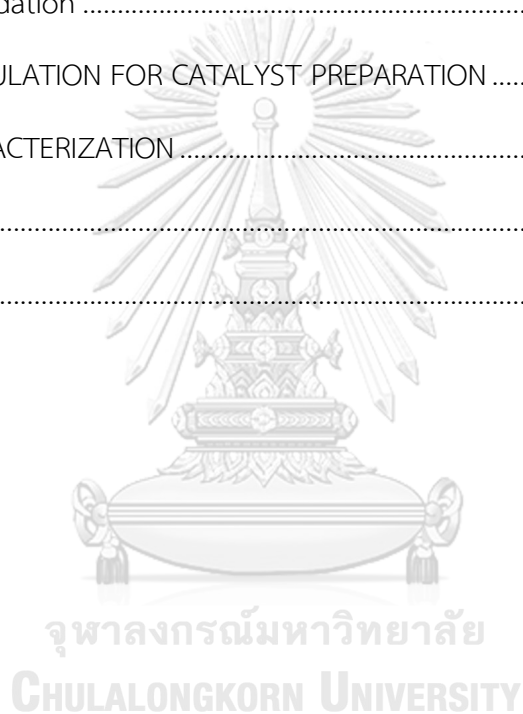
Kanokpon Maungthong

TABLE OF CONTENTS

	Page
ABSTRACT (THAI).....	iii
ABSTRACT (ENGLISH).....	iv
ACKNOWLEDGEMENTS.....	v
TABLE OF CONTENTS.....	vi
LIST OF TABLES.....	ix
LIST OF FIGURES.....	xi
CHAPTER I.....	1
INTRODUCTION.....	1
1.1 Introduction.....	1
1.2 Objective.....	4
1.3 The scope of the research.....	4
1.4 Research methodology.....	6
CHAPTER II BACKGROUND AND LITERATURE REVIEWS.....	7
2.1 Methyl oleate.....	7
2.2 Methyl 9,10-epoxy stearate.....	8
2.3 Epoxidation reaction.....	9
2.3.1 Temperature.....	12
2.3.2 Reaction time.....	14
2.3.3 Solvent.....	15
2.3.4 Oxidizing reagent.....	18
2.4 Catalysts and literature reviews.....	19

2.4.1 TiO ₂ (P25).....	21
2.4.2 Titanosilicate (TS-1).....	24
2.4.3 Gamma alumina (γ -Al ₂ O ₃).....	26
2.5 Deactivation of catalyst.....	30
CHAPTER III EXPERIMENTAL	33
3.1 Materials and chemicals.....	33
3.2 Catalyst Preparation	34
3.2.1 TiO ₂ (P25).....	34
3.2.2 γ -Al ₂ O ₃	34
3.2.3 Titanosilicate (TS-1).....	34
3.3 Catalytic activity test on the epoxidation reaction.....	35
3.4 Catalyst Characterization.....	37
3.4.1 X-ray diffraction (XRD).....	37
3.4.2 X-ray photoelectron spectroscopy (XPS).....	37
3.4.3 Ultraviolet-visible spectrophotometry (UV-vis).....	38
3.4.4 Temperature programmed oxidation (TPO).....	38
3.4.5 Fourier-transform infrared spectroscopy (FT-IR).....	38
3.4.6 Inductively coupled plasma - optical emission spectrometry (ICP-OES)..	38
CHAPTER IV RESULTS AND DISCUSSION	39
4.1. Deactivation of P25, TS-1, γ -Al ₂ O ₃ during the MO Epoxidation	39
4.1.1. Investigation the deactivation rate on the P25, TS-1, γ -Al ₂ O ₃	39
4.1.2. The fouling deposits on the P25, TS-1, and γ -Al ₂ O ₃ surfaces.....	42
4.1.3. The oxygen vacancy on the surface	45
4.1.4. The leaching effect	49

4.2. Regeneration of P25, TS-1, γ -Al ₂ O ₃ after the MO Epoxidation.....	50
4.2.1. Investigation the catalytic activity after the regeneration	50
4.2.2. The effect of phase structure and crystallinity of catalyst	51
4.2.3. Analysis on the regeneration of TS-1 surface	54
CHAPTER V CONCLUSIONS AND RECOMMENDATIONS	59
5.1. Conclusions	59
5.2. Recommendation	60
APPENDIX A CALCULATION FOR CATALYST PREPARATION	62
APPENDIX B CHARACTERIZATION	65
REFERENCES	68
VITA.....	76



LIST OF TABLES

	Page
Table 1 Fatty acid compositions (wt. %) of palm oil [3].....	2
Table 2 Physical and chemical properties of methyl oleate [16].....	8
Table 3 Physical and chemical properties of methyl 9,10-epoxy stearate [15].....	9
Table 4 Effect of Temperature on Epoxidation of Methyl linoleate (M_L) [19].....	13
Table 5 Influence of the solvent on initial rate of reaction, conversion of methyl oleate X_{MO} , selectivity S_{ME} and conversion of hydrogen peroxide $X_{H_2O_2}$ in the epoxidation of methyl oleate over TS-1 (ind.) at 50 °C after 24 h [11].....	15
Table 6 Operating conditions adopted for the epoxidation reaction at 80 °C and related conversion and selectivity results [14].....	16
Table 7 Properties of solvents [23].....	18
Table 8 Screening heterogeneous catalysts on the epoxidation reaction	19
Table 9 Screening heterogeneous catalysts on the epoxidation reaction [37]	21
Table 10 Varying the calcination temperature to know the phase transformation [50]	28
Table 11 Chemicals used in epoxidation reaction and catalyst preparation.....	33
Table 12 Crystallite size and the crystallinity of fresh catalysts	41
Table 13 XPS data of different oxidation state of Ti and O on the surface of TiO_2 (P25) and titanosilicate (TS-1) where O_L represents the lattice oxygen, O_S represents the sub oxide, and O_V represents the oxygen vacancies.....	46
Table 14 Concentration of metal oxide in the liquid samples by ICP-OES measurement	50
Table 15 Crystallite size and the crystallinity of P25 and TS-1 catalysts after the regeneration at 550 °C and 700 °C calculated by Scherrer equation	53

Table 16 XPS data of different oxidation state of Ti and O on the surface of fresh, spent, and regenerated titanosilicate (TS-1) where O_L represents the lattice oxygen, O_S represents the sub oxide, and O_V represents the oxygen vacancies. 58



LIST OF FIGURES

	Page
Figure 1. Reaction pathway for the epoxidation of alkene [9]	3
Figure 2. Chemical structure of methyl oleate [6]	7
Figure 3. Chemical structure of methyl 9,10-epoxy stearate [6].....	8
Figure 4. Epoxidation reaction of methyl oleate	9
Figure 5. Proposed reaction scheme for the epoxidation of MO with H ₂ O ₂ on TS-1 [6]	10
Figure 6. Reaction pathway for the oxidation with H ₂ O ₂ catalyzed by acids [10].....	11
Figure 7. Effect of temperature on reaction rate and selectivity at 0.4 MPa [18].....	12
Figure 8. Effect of reaction temperature on conversion of methyl oleate X _{MO} and epoxide selectivity S _{ME} in the epoxidation of methyl oleate over TS-1 [11].....	13
Figure 9. Conversion and selectivity as a function of reaction time in epoxidation reaction of methyl oleate epoxide over TS-1 [11].....	14
Figure 10. MO and H ₂ O ₂ conversion obtained for TN/CLO _{4p} 0.01 sample tested with various initial amounts of H ₂ O ₂ at 25 °C and 40 °C [24].....	19
Figure 11. TiO ₂ crystal structures: rutile (a), anatase (b) and brookite (c) [37].....	22
Figure 12 XRD patterns of the TiO ₂ catalysts calcined at various temperatures [39] ..	22
Figure 13. Reaction scheme for the epoxidation of cyclohexene via the allylic oxidation (up) or the direct epoxidation routes (bottom) [13].....	23
Figure 14. The structure of the orthorhombic form of silicalite (MFI-type).....	24
Figure 15. XRD patterns of HZ, P-HZ, Fe-HZ and Fe-P-HZ [40-42]	25
Figure 16. Mechanism of the titanosilicate epoxidation catalysts in the water [13]. ...	26
Figure 17. Gamma aluminium oxide [48].....	27

Figure 18. Boehmite dehydration and phase transition route in the Al_2O_3 system [49]	27
Figure 19. XRD patterns for the produced alumina membranes by heating boehmite at 450–1300°C for 0.5 h. [53]	29
Figure 20 Proposed mechanism of the epoxidation and oxygen formation [54].	30
Figure 21 Catalytic activity test in the MO epoxidation over TS-1 (ind.) at 323 K (left part) and reuse or regeneration (RC: regenerated catalyst, calcination in air flow for 6 h at 823 K) of the catalyst (right part) [11].	30
Figure 22. Synthesis of titanosilicate (TS-1) by hydrothermal method	34
Figure 23. Epoxidation reaction of methyl oleate	35
Figure 24. Temperature program of GC-MS condition	37
Figure 25. The reusability testing in a 50 cm ³ three-necked round-bottom glass reactor during MO epoxidation with H_2O_2 over difference catalysts at 50 °C for 5 h..	40
Figure 26 Thermal gravimetric analysis (TGA) of used P25, TS-1, and $\gamma\text{-Al}_2\text{O}_3$ catalysts	42
Figure 27. Temperature program oxidation (TPO) plots of used P25, TS-1, and $\gamma\text{-Al}_2\text{O}_3$ catalysts	43
Figure 28. Fourier transform infrared spectroscopy (FT-IR) of before (a1) and after (a2) reaction of P25, TS-1, and $\gamma\text{-Al}_2\text{O}_3$ catalysts	44
Figure 29 The high resolution XPS spectra of Ti2p in the fresh and deactivated of (a, b) P25 and (c, d) TS-1 Ti-based catalysts	47
Figure 30 The high resolution XPS spectra of O1s in the fresh and deactivated of (a, b) P25 and (c, d) TS-1 Ti-based catalysts	47
Figure 31 (a) UV spectroscopy profile of (I) fresh P25, (II) 2 nd run of P25, and (III) 3 rd run of P25 catalysts (b) TUAC relation plot of (I) fresh P25, (II) 2 nd run of P25, and (III) 3 rd run of P25 catalysts	48

Figure 32. (a) UV spectroscopy profile of (I) fresh TS-1, (II) 2 nd run of TS-1, and (III) 3 rd run of TS-1 catalysts a (b) TUAC relation plot of (I) fresh TS-1, (II) 2 nd run of TS-1, and (III) 3 rd run of TS-1 catalysts.....	48
Figure 33. The MO conversion of P25, TS-1, and γ -Al ₂ O ₃ catalysts through the MO epoxidation reaction with variation of calcination temperature.....	51
Figure 34. XRD patterns of fresh P25 and regenerated P25 with difference calcination temperature (550 °C and 700 °C).....	52
Figure 35. XRD patterns of fresh TS-1 and regenerated TS-1 with difference calcination temperature (550 °C and 700 °C).....	52
Figure 36. XRD patterns of fresh γ -Al ₂ O ₃ and regenerated γ -Al ₂ O ₃ with difference calcination temperature (550 °C and 700 °C).....	53
Figure 37. The MO conversion and ME selectivity of fresh TS-1, spent TS-1, and regenerated TS-1 catalysts at 550 °C via MO epoxidation in a 50 cm ³ batch reactor at 50 °C.....	54
Figure 38. Temperature program oxidation profile of fresh TS-1, spent TS-1, and regenerated TS-1 catalysts.....	55
Figure 39 Ti2p XPS spectra of (a) fresh TS-1, (b) spent TS-1, and (c) regenerated TS-1.....	57
Figure 40. O1s XPS spectra of (a) fresh TS-1, (b) spent TS-1, and (c) regenerated TS-1.....	57
Figure 41. (a) UV spectroscopy profile of (I) fresh TS-1, (II) spent TS-1, and (III) regenerated TS-1 catalysts (b) TUAC relation plot of (I) fresh TS-1, (II) spent TS-1, and (III) regenerated TS-1 catalysts.....	57

CHAPTER I

INTRODUCTION

1.1 Introduction

Nowadays, fossil and petroleum feedstocks are the exhaustible natural resources which have been depleted by increasing demands of human. The diminishing fossil sources result in the shortage of natural resources, therefore the renewable feedstocks are interesting to replace the limited natural resources. Moreover, the chemical industry has been shifting towards greener technologies to reduce environmental pollution. Also, biomass is one of the best choices for a sustainable feedstock to use as a raw material for chemical production. Currently, palm oil has played an important role as a renewable feedstock to produce food and global energy in Thailand because Thailand is the center of Southeast Asia to generate and trade of palm oil up to 45 percent of the world's production. In recent years, the oversupply and decline in the price of the palm oil in Southeast Asia market are founded due to world economic growth slowest. Therefore, the conversion of palm oil to a high value product is interesting [1]. Palm oil has high capacity to produce FAME via the transesterification of vegetable and animal oils by using acid catalyst [2].

Ramos et al. (2009) was studied the fatty acid composition of raw materials on biodiesel properties as shown in Table 1. Oleic compound (C: 18) was founded 46.1 wt. % of the palm oil as the major component [3]. For the applications of FAME, the epoxidation reaction is concerned to produce the epoxy products because the catalytic activity and selectivity of desired products were higher for epoxidation reaction at the low temperature. The reaction converted the unsaturated double bonds fatty acid methyl ester to oxirane ring or epoxide with a peracid or peroxyacid as shown in Figure 1 [4]. Epoxy products are used in many fields such as plasticizers [5], stabilizer in PVC, intermediates in polyurethane polyols, lubricants [6], cosmetics, precursors of various polymer [7], wood impregnation, biofuel additives, and pharmaceuticals [8].

Table 1 Fatty acid compositions (wt. %) of palm oil [3]

Properties		Information
Lauric	C12:0	0.1
Myristic	C14:0	0.7
Palmitic	C16:0	36.7
Palmitoleic	C16:1	0.1
Stearic	C18:0	6.6
Oleic	C18:1	46.1
Linoleic	C18:2	8.6
Linolenic	C18:3	0.3
Arachidic	C20:0	0.4
Gadoleic	C20:1	0.2
Behenic	C22:0	0.1
Erucic	C22:1	0.0

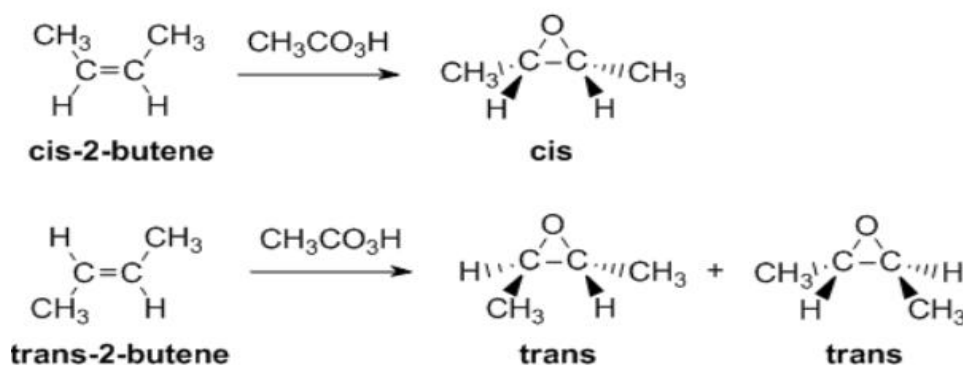


Figure 1. Reaction pathway for the epoxidation of alkene [9]

For industrial scale, the Prileshajew reaction is carried out on the epoxidation reaction in liquid phase at the low temperature. Homogeneous catalysts are performed by soluble mineral acids such as H₃PO₄, HCl or H₂SO₄. The active site as the peracid molecule can be promoted by the oxidizing reagent as the hydrogen peroxide, however it produces only water as a by-product [9]. The oxygen atom of the peracid is attacked at the double bond of an unsaturated fatty acids methyl ester to form the epoxide [10]. Although the homogeneous catalyst provide the high catalytic activity on the epoxidation reaction, it has mainly three drawbacks in the homogeneous process. The first drawback is the toxicity of the substrate such as peracid and highly concentrated hydrogen peroxide. The second drawback is the corrosion of the C1-C3 carboxylic acids. And the final drawback is the limitation of the homogeneous catalyst which is difficult separation and low selectivity [11, 12]. In addition, the homogeneous catalyst also cannot re-use and regenerate easily. Consequently, the heterogeneous catalyst is interesting to catalyze via the epoxidation instead of the homogeneous catalyst because it's easy to separate and regenerate including high selectivity.

From those drawbacks, we focus on the heterogeneous catalyst used via the epoxidation reaction in the liquid phase. Ti-based catalysts are concerned especially titanium dioxide (TiO₂, P25) and titanosilicate (TS-1) because these catalysts are the general commercial catalyst and the combination of Ti-based catalyst with hydrogen peroxide give the higher catalytic conversion and selectivity. The silica molecule promote the dispersion of TiO₂ which affect to the conversion of alkene [13]. Moreover, gamma alumina is also dominated on the epoxidation reaction same as the Ti-based

catalysts. Both of Ti-based catalysts and gamma alumina are catalyzed the epoxidation reaction via the hydroperoxo molecule (X-OOH) as the active site [14]. In addition, the γ - Al_2O_3 performs the hydroperoxo molecule as the Al-OOH sites that active on the epoxidation reaction too. However, the heterogeneous catalysts mostly show the low stability for the chemical reaction due to catalyst deactivation. To achieve the highest performance of such heterogeneous catalysts and to eliminate some drawback of heterogeneous reaction as a low stability, one must tackle the main issue concerning the deactivation and regeneration by understanding the defects on the surface for spent catalysts.

Due to the lacking of deactivation for the epoxidation, this project investigates the deactivation scheme and surface of TiO_2 (P25), TS-1 as the Ti-based catalysts, and γ - Al_2O_3 during the liquid phase epoxidation reaction of methyl oleate with hydrogen peroxide at low temperature.

1.2 Objective

To investigate the deactivation scheme and surface on P25, TS-1 as the Ti-based catalysts, and γ - Al_2O_3 during the liquid phase epoxidation reaction of methyl oleate at low temperature.

1.3 The scope of the research

The epoxidation of methyl oleate were tested at temperature of 50 °C and atmospheric pressure. Hydrogen peroxide (H_2O_2) was used as the oxidizing reagent and acetonitrile was used as the solvent. The commercial of P25 and γ - Al_2O_3 were obtained. The deactivated catalysts were centrifuged and run the reaction again. There are 4 scopes of research given below.

1.3.1. Titanosilicate (TS-1) was prepared by the hydrothermal method.

1.3.2. Catalytic activity and selectivity of desired product were analyzed by gas chromatography apparatus equipped with the mass spectrometric detector and the DB-5 column (GC-MS).

1.3.3. The spent catalysts were regenerated by various calcination temperatures of 550 °C and 700 °C

1.3.4. The fresh, spent, and regenerated catalysts were characterized by different analytical techniques. There are 5 techniques as follows;

1.3.4.1 X-ray diffraction (XRD) to observe the structure and phase changing after the MO epoxidation reaction

1.3.4.2 X-ray photoelectron spectroscopy (XPS) to examine the oxidation states of Ti and O species on the surface including the oxygen vacancy (O_V)

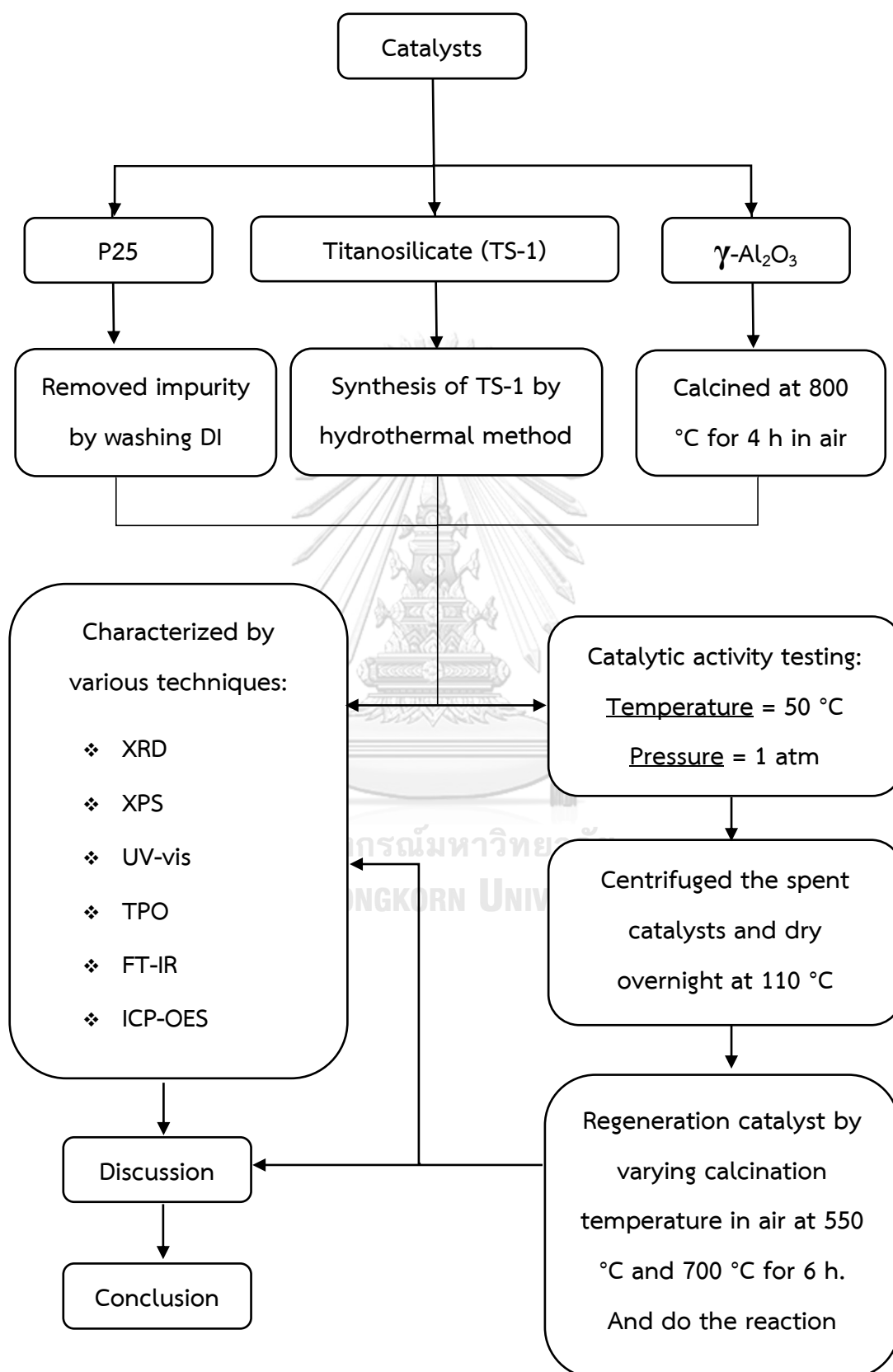
1.3.4.3 Ultraviolet–visible spectrophotometry (UV–Vis) to investigate the energy gap by the adsorption versus energy profiles to confirm oxygen vacancy (O_V)

1.3.4.4 Temperature programmed oxidation (TPO) to verify the functional group of fouling deposits on the surface catalysts after the MO epoxidation reaction

1.3.4.5 Fourier-transform infrared spectroscopy (FT-IR) to investigate the functional group of fouling deposits on the surface catalysts after the MO epoxidation reaction

1.3.4.6 Inductively coupled plasma - optical emission spectrometry (ICP-OES) to investigate the leaching effect from the liquid solution after the reaction

1.4 Research methodology



CHAPTER II

BACKGROUND AND LITERATURE REVIEWS

This chapter concern the background knowledge and the literature review to describe the information of methyl oleate as the feedstock and methyl 9,10-epoxy stearate as the desired product. In addition, it shows the detail of epoxidation reaction and catalyst reviewing via the epoxidation reaction below.

2.1 Methyl oleate

Methyl oleate (MO) is a one kind of the fatty acid methyl ester (FAMES) that produces by the tranesterification reaction of oils and fats from the vegetable. It is an organic chemical compound that constituent of palm oil and have the number of hydrocarbon highly. IUPAC name of methyl oleate is methyl-(9Z)-9-octadecenoat and the other names are 9-Octadecenoic acid, Oleic acid methyl ester, or Methyl cis-9-octadecanoate. The chemical formula is $C_{19}H_{36}O$ as shown in Figure 2. There are many applications for methyl oleate as intermediate for detergents, wetting agents, stabilizers, textile treatments, plasticizers for duplicating inks, rubbers and waxes. The physical and chemical properties are listed in the Table 2 [15].



Figure 2. Chemical structure of methyl oleate [6]

Table 2 Physical and chemical properties of methyl oleate [16]

Properties	Information
Formula	$C_{19}H_{36}O_2$
Molecular weight	296.49 g/mol
Form	Oily liquid
Color	Clear yellow to amber
Density	0.874 g/mL at 20 °C
Melting point	-20°C
Boiling point	218 °C at 20 mm Hg
Storage temp.	-20°C

2.2 Methyl 9,10-epoxy stearate

Methyl 9,10-epoxy stearate is the desired product of the epoxidation reaction by using the methyl oleate as the raw material. IUPAC name of Methyl 9,10-epoxy stearate is methyl 8-(3-octyl-2-oxiranyl) octanoate and the other names are 2-oxiraneoctanoic acid, palmitinsaeure-dimethylami, and 9,10-epoxystearic acid methyl ester. Methyl 9,10-epoxy stearate is an organic compound that have the number of hydrocarbon highly and contain an oxirane ring between the carbon atom of 9-10 as shown the chemical structure in Figure 3. The chemical formula is $C_{19}H_{36}O_3$ [15]. There are many applications of methyl 9,10-epoxy stearate as the additive for lubricants, intermediates in polymer (polyurethane) [6], plasticizer in the PVC production [5], and intermediates in the pharmaceutical industry.

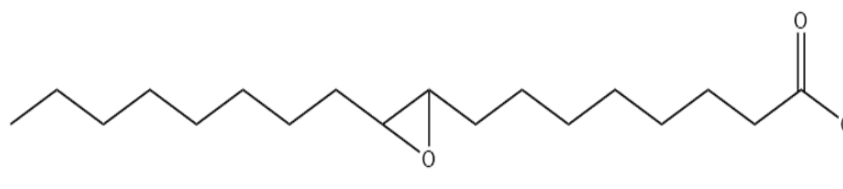
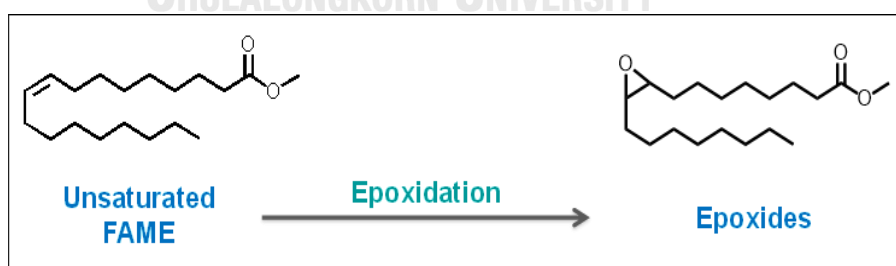
**Figure 3.** Chemical structure of methyl 9,10-epoxy stearate [6]

Table 3 Physical and chemical properties of methyl 9,10-epoxy stearate [15]

Properties	Information
Formula	$C_{19}H_{36}O_3$
Molecular weight	312.49 g/mol
Form	Liquid
Color	Clear white
Density	0.925 g/mL at 20 °C
Melting point	15-16.5 °C
Boiling point	161-163 °C at 0.064 Torr
Price/unit	28.5 USD/ 1g

2.3 Epoxidation reaction

Nowadays, there are many methods to upgrade the FAMEs to high-value product. One of method is the epoxidation reaction to change the methyl ester to the epoxy group. This reaction is very interesting because it gives the high conversion and selectivity for heterogeneous catalyst [16]. Therefore, we will select the methyl oleate as the renewable raw material to generate the epoxy product as shown in Figure 4.

**Figure 4.** Epoxidation reaction of methyl oleate

Wilde et al. (2012) investigated the epoxidation of biodiesel with hydrogen peroxide over Ti-containing silicate catalysts. It reported the general epoxidation description. The double bond could be converted to the oxirane ring by using the heterogeneous catalyst with the hydrogen peroxide. The intermediate of Ti-OOH as the active site was formed by the hydrogen peroxide which reacted to the tetrahedral Ti [11].

Yang et al. (2008) observed green and efficient epoxidation of methyl oleate over hierarchical TS-1. The proposed mechanism of epoxidation reaction was shown in Figure 5. The main reaction was the direct epoxidation and allylic oxidation with hydrogen peroxide to form the epoxy product and get the molecule of water as the by-products. The direct epoxidation was occurred via the intermediate of Ti-OOH and the allylic oxidation was occurred via the intermediate of TiO· radical. For side reaction, there are 3 pathways to open the oxirane ring. The first reaction was the oxidative rearrangement to get the ketone molecule. The hydrolysis and oxidative cleavage reactions were observed under the acidic conditions to get the undesired products. The hydrolysis was the major side reaction to affect the low selectivity of epoxy product [6].

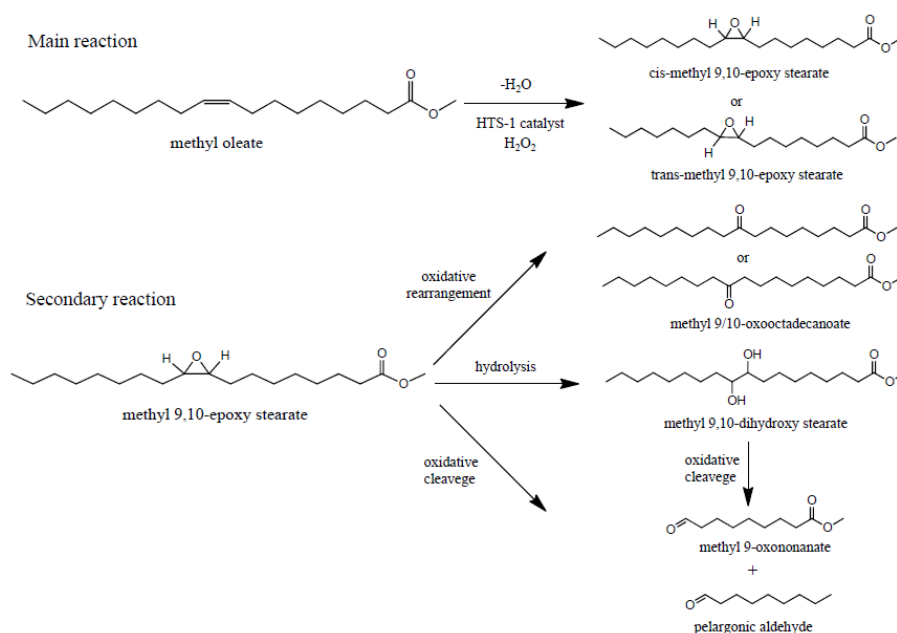


Figure 5. Proposed reaction scheme for the epoxidation of MO with H_2O_2 on TS-1 [6]

Turco et al. (2016) investigated the new findings on soybean and methyl ester epoxidation with alumina as the catalyst. It's reported the presence of water affected the selectivity of oxirane ring because the water promoted the hydrolysis as the side reaction to form the dio-molecule. Moreover, H_2O_2 could be decomposed between the reaction to loss the catalytic activity and increase the amount of water [14, 17]. Consequently, the selectivity of epoxy product was depended on the amount of water and H_2O_2 decomposition.

On the industry scale, the epoxidation was carried out with the Prileschajew reaction which used the homogeneous catalyst commonly such as H_3PO_4 , HCl or H_2SO_4 . The reaction pathway was shown in Figure 6. The unsaturated oils reacted with a percarboxylic acid such as peracetic [10] and performic acid, obtained via the acid-catalyzed oxidation of the respective organic acid with hydrogen peroxide as the oxidant to form the oxirane ring. However, an excess of hydrogen peroxide and acetic acid promoted the ring opening reaction [10].

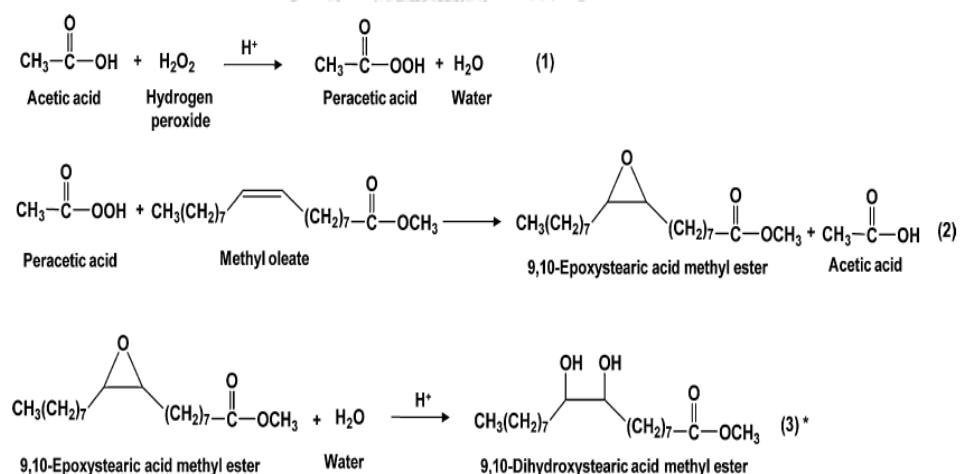


Figure 6. Reaction pathway for the oxidation with H_2O_2 catalyzed by acids [10]

Although the acidity and selectivity via Prileschajew reaction are high, it have some drawbacks as follow. 1) The sample is difficult to separate and neutralize from the strong acid catalyst. 2) The system is toxic and corrosive with the equipment. 3) The homogeneous catalyst cannot regenerate and reuse. Therefore, the heterogeneous

catalyst is interesting. Hydrogen peroxide is used as oxidants because it produces only water as the by-product [6, 10].

2.3.1 Temperature

Wu et al. (2013) explained on the epoxidation of propylene with H_2O_2 catalyzed by supported TS-1 catalyst in a fixed-bed reactor to study the experimental and kinetic model as shown in Figure 7. The results showed the catalytic activity and selectivity depended on both temperature and pressure. The reaction rate increased with the rising temperature at 50 °C, but the selectivity of propylene oxide as a desired product (PO) decreased. In addition, the selectivity of alkyl ethers (MME) as an undesired product was constant [18]. Correspondingly, M. You (2016) was optimized the condition of epoxidation reaction by using unsaturated fatty acid methyl esters and vegetable oils especially temperature as shown in Table 4. The selectivity of epoxide is decreased when the temperature is higher than 25 °C for heterolytic pathway [19, 20]. Figure 8 shows the optimum temperature is 50 °C because the selectivity is slightly affected by temperature up to 60 °C [11].

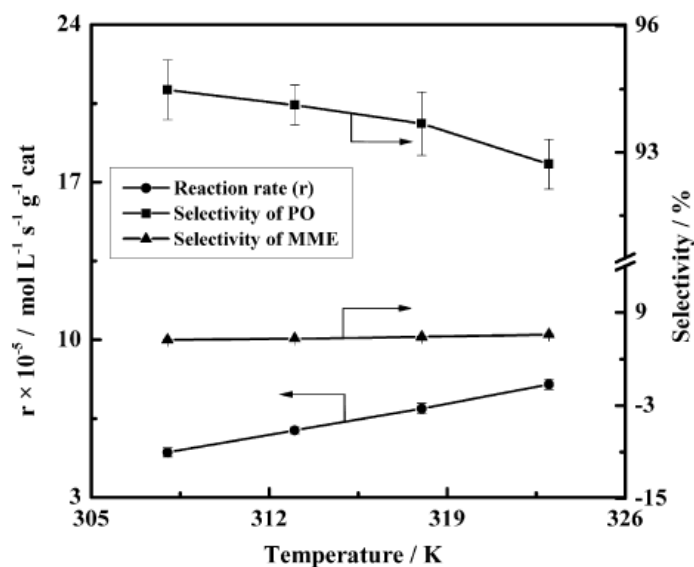


Figure 7. Effect of temperature on reaction rate and selectivity at 0.4 MPa [18]

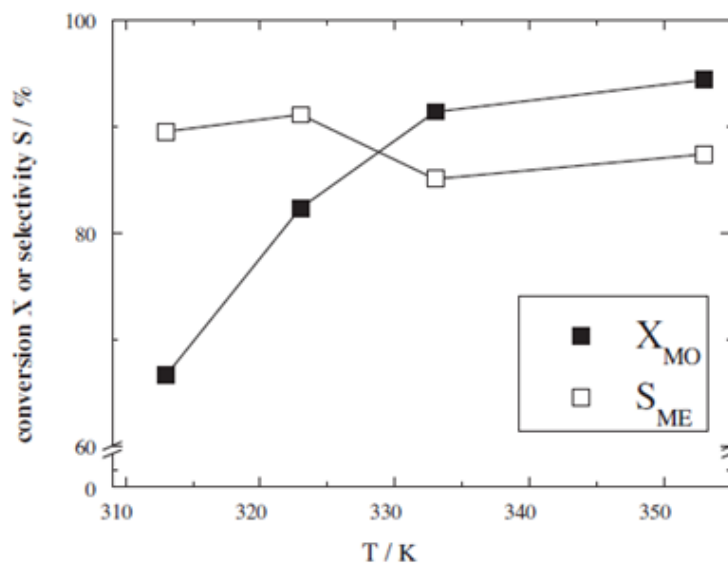


Figure 8. Effect of reaction temperature on conversion of methyl oleate X_{MO} and epoxide selectivity S_{ME} in the epoxidation of methyl oleate over TS-1 [11].

Table 4 Effect of Temperature on Epoxidation of Methyl linoleate (M_L) [19]

Entry	T (°C)	Conversion (%)	Monoepoxide (%)	Diepoxide (%)	Total epoxide (%)
1	5	77.8	28.7	49.3	63.7
2	15	84.3	15.1	59.2	66.8
3	25	100.0	4.7	90.4	92.8
4	35	100.0	2.5	87.9	89.2
5	45	100.0	0.0	82.1	82.1

2.3.2 Reaction time

Wilde et al. (2012) tested the conversion and selectivity as a function of reaction time on the epoxidation of biodiesel with H_2O_2 catalyzed by supported TS-1 catalyst at 50 °C. For the first 5 h, the methyl oleate (MO) and H_2O_2 conversions were risen rapidly. However, the reaction time was varied with the epoxide (ME) selectivity inversely because H_2O_2 could be degraded to H^+ and water (H_2O) which promoted the oxirane ring opening as the side reaction [11]. After the 5 h, titanium could be leached during the reaction. It affected to the decreasing of active site and got the low conversion respectively [21]. Consequently, the optimum reaction time was 5 h because this condition got the optimum of both conversion and selectivity as shown in Figure 9.

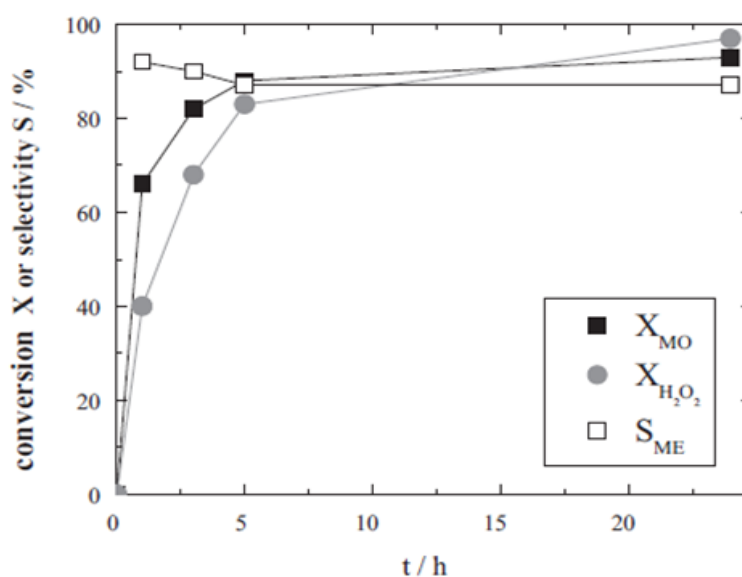


Figure 9. Conversion and selectivity as a function of reaction time in epoxidation reaction of methyl oleate epoxide over TS-1 [11].

2.3.3 Solvent

Wilde et al. (2012) investigated on the effect of solvent via the epoxidation reaction of biodiesel with hydrogen peroxide over Ti-containing silicate catalysts. The catalytic activity and selectivity were examined by varying the solvent as shown in Table 5. The homogeneous solution promoted highly efficiency of the epoxidation reaction. Therefore, the nature of solvents and substrates were influence on the solubility of the reactant mixture [11, 22]. The solubility was dominated property because the solubility of FAMES and oils in hydrogen peroxide solution was limited. According to Table 5, the effect of polarity and the protic/aprotic nature of different solvents affected on initial reaction rate, conversion of MO and H₂O₂ and epoxide selectivity. The aprotic-polar solvents like ethyl acetate provided the highest MO conversion of 90%, however the ME selectivity were below 50% [11].

Table 5 Influence of the solvent on initial rate of reaction, conversion of methyl oleate X_{MO} , selectivity S_{ME} and conversion of hydrogen peroxide $X_{H_2O_2}$ in the epoxidation of methyl oleate over TS-1 (ind.) at 50 °C after 24 h [11].

Solvent	Initial rate r_0 (mol l ⁻¹ h ⁻¹)	Conversion X_{MO} (%)	Selectivity S_{ME} (%)	Conversion $X_{H_2O_2}$ (%)
Ethylacetate	0.025	98	36	72
Acetone	0.024	92	52	36
Acetonitrile	0.021	93	87	97
Acetonitrile/methanol	0.016	79	85	62
Diglyme	0.015	79	84	66
Methanol	0.002	20	17	57
Diisopropylether	0.005	4	31	67

Turco et al. (2016) also examined on the effect of solvent via the epoxidation reaction of vegetable oils and their derivatives such as soybean oil on gamma alumina by using hydrogen peroxide. The solubility was dominated property because the solubility of FAMES and oils in hydrogen peroxide solution was limited. Moreover, the solubility depended on the types of substrates and solvents. According to Table 6, acetic acid was detected in the sample mixture after the epoxidation reaction, in the presence of ethyl acetate as solvent. It promoted the peracetic acid to form many active site (Al-OOH), however acetic acid could enhanced the oxirane ring opening reaction to affect the selectivity. Acetonitrile could be provided high conversion and selectivity due to homogeneous solution when mixed with the oil including acetonitrile could be filled most of pore volume of catalyst. Methanol and toluene could not dissolve the oil to affect the low conversion and selectivity [14]. To compare the polarity and solubility of different solvent, acetonitrile is suitable for methyl ester such as methyl oleate because the high polarity of acetonitrile ($\epsilon = 36$) as shown in Table 7 [23].

Table 6 Operating conditions adopted for the epoxidation reaction at 80 °C and related conversion and selectivity results [14]

Run	Substrate	Solvent	H ₂ O ₂ (g)	Substrate (g)	Alumina (g)	time (h)	MO Conversion (%)	ME Selectivity (%)
1	Soybean oil	Ethyl acetate	6.9	5.0	0.6	5	56	59
2	Soybean oil	Ethyl acetate	6.9	5.0	0.6	10	75	64
3	-	Ethyl acetate	6.9	-	0.6	5	78 ^a	-
4	Soybean oil	Ethyl acetate	6.9	5.0	-	5	0	-

5	-	Ethyl acetate	6.9	-	0.6	2.5	65 ^a	-
6	Soybean oil	Solution of Run 5	-	5.0	-	2.5	11	41
7	Soybean oil	Ethyl acetate	6.9	5.0	0.6	5	57	71
8	Soybean oil	Acetonitrile	6.9	5.0	0.6	5	72	81
9	Soybean oil	Toluene	6.9	5.0	0.6	5	22	7.0
10	Soybean oil	Acetonitrile	6.9	5.0	0.6	5	6.7	4.3
11	-	Acetonitrile	6.9	-	0.6	2.5	-	-
12	Soybean oil	Solution of Run 11	-	5.0	0.6	2.5	0	-
13	Soybean oil	Acetonitrile	6.9	5.0	0.6	5	75	58
14	Soybean oil	Acetonitrile	6.9	5.0	0.6	8	71	74
15	Soybean oil	Acetonitrile	8.1	5.0	0.6	5	70	77
16	Soybean oil	Acetonitrile	6.9 + 3.4	5.0	0.6	8	80	96

Table 7 Properties of solvents [23]

	Solvent	Boiling point (°C)	Diploe moment (10^{-30} C m)	Dielectric constant at 20 °C	Polarity index
Protic	Methanol	64.7	5.67	33	6.6
	Ethanol	78.3	5.64	26	5.2
	Isopropanol	82.3	5.30	20	3.9
	1,2-Propanediol	188	7.34	32	-
	Water	100	6.15	81	9.0
Polar aprotic	N,N-dimethylformamide	153	12.7	37	6.4
	Acetonitrile	81.6	13.1	36	6.2
	Benzonitrile	191	13.1	25	4.6
Apolar aprotic	Diisopropyl ether	68.5	4.20	3.8	2.4
	Ethyl acetate	77.1	5.94	6.0	4.3
	n-Hexane	69.0	0	1.9	0.1

2.3.4 Oxidizing reagent

Pajić et al. (2018) analyzed the effect of active peroxy species on TiO₂-nanotube via the epoxidation reaction as shown in Figure 10. The optimum molar ratio of methyl oleate (MO) and hydrogen peroxide (H₂O₂) was 1:2 at the temperature of 40 °C to produce the highest hydroperoxy group (TI-OOH) as the active site of the epoxidation reaction and to give the highest H₂O₂ consumption. MO conversion increases slightly for TN/CLO₄p 0.01 sample from 74% with stoichiometric H₂O₂ amount to 89% MO conversion with double stoichiometric amount of H₂O₂ corresponding to TiO₂-nanotube [24].

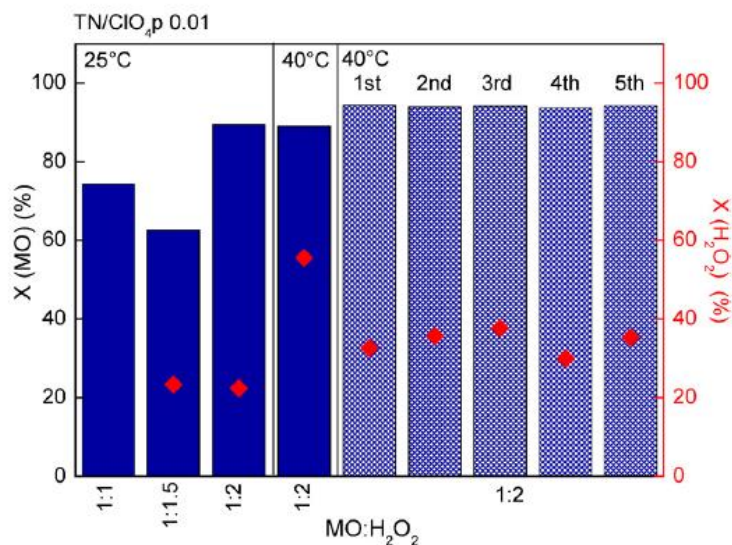


Figure 10. MO and H₂O₂ conversion obtained for TN/ClO_{4p} 0.01 sample tested with various initial amounts of H₂O₂ at 25 °C and 40 °C [24].

2.4 Catalysts and literature reviews

Generally, the catalysts were important for catalytic chemical reaction as the epoxidation reaction. There are 2 kinds of catalysts like the homogeneous and heterogeneous catalysts. Heterogeneous catalysts were focused to solve the drawbacks of homogeneous catalysts. Table 8 showed the heterogeneous catalyst screening on the epoxidation reaction for laboratory and industrial scale below:

Table 8 Screening heterogeneous catalysts on the epoxidation reaction

Catalyst	Substrate	Solvent	T (°C)	Reference
TiO ₂ Ti/SiO ₂	Propylene	-	80	[25]
TS-1 Ti-MCM-41	1-Hexene, Cyclohexene, Cyclooctene, and Cyclododecene	Acetonitrile	60	[26]

Ti-SBA 15	Cyclohexane	Benzonitrile	60	[27]
TS-1 Ti-MCM-41 TiO _x -SiO ₂ WO _x -Al ₂ O ₃ MoO _x -Al ₂ O ₃ MoO _x -SiO ₂	Methyl oleate	Acetonitrile	50	[11]
Mn/Ti-MCM-41	Cyclohexene	Acetonitrile	80	[28]
Co-MOF	Cyclooctene	Acetonitrile	35	[29]
CoO _x CoO _x /SiO ₂	Cis-cyclooctene	DMF	120	[30]
Au/TiO ₂	Stilbene	Methylcyclohexane	80	[31]
GaO _x Al-MCM-41 Ga-MCM-41 Zeolite	Cyclooctene	Acetonitrile	25	[32]
MeReO ₃	Alkene	Trifluoroethanol	25	[33]
Pd/UIO-66-NH ₂	Styrene	Ethanol, Methanol	40 - 80	[34]
Peroxo- phosphotungstic	dicyclopentadiene	Acetonitrile	50	[35]
γ-Al ₂ O ₃	Methyl oleate	Ethyl acetate	80	[14]

For this research, we focused on the commercial catalysts because it's easy to trade and use in industrial scale. To investigate the deactivation scheme and the stability of these catalysts as shown in Table 8. We can categorize the catalyst by varying the different structure such as crystalline structure (P25), well-defined structure (TS-1), and amorphous (γ-Al₂O₃).

2.4.1 TiO₂ (P25)

Titanium dioxide (TiO₂) is the one of common materials to select in the many field of industry, being used in architecture industry and automotive coatings; furniture, electrical appliances including the paint pigment, fiber, synthetic rubber, filter coating cosmetics, catalysts, and so on. TiO₂ can be used variously because it has many excellent properties including low density, high temperature resistance, low temperature resistance, non-toxicity, high chemical stability, low cost, and anti-corrosion properties [36]. They are 3 main crystalline forms for normal TiO₂ like anatase (tetragonal), rutile (tetragonal), and brookite (orthorhombic) as shown in Table 9 and Figure 11. Anatase and rutile are the most common natural form of TiO₂. They form the tetragonal structure as the needle crystalline-like structure. Brookite as orthorhombic form is found infrequently form of the mineral, and is not easily obtained. In addition, brookite has the lower activity than anatase and rutile because generally the active site is the tetragonal or tetrahedral structure. Rutile has the lower free energy than anatase and brookite depending on the presence of impurities, the size of the particles [37]. Anatase is the structure that commonly used in the photocatalytic reaction because the crystal system shows the dipyramidal habit which promotes the activity for photocatalyst [38].

Table 9 Screening heterogeneous catalysts on the epoxidation reaction [37]

	Crystal system	Density (g/cm ³)	Optical band-gap	Refractive index
Rutile	Tetragonal	4.13-4.26	3.0	2.72
Anatase	Orthorhombic	3.99-4.11	3.11	2.63
Brookite	Tetragonal	3.79-3.84	3.19	2.52

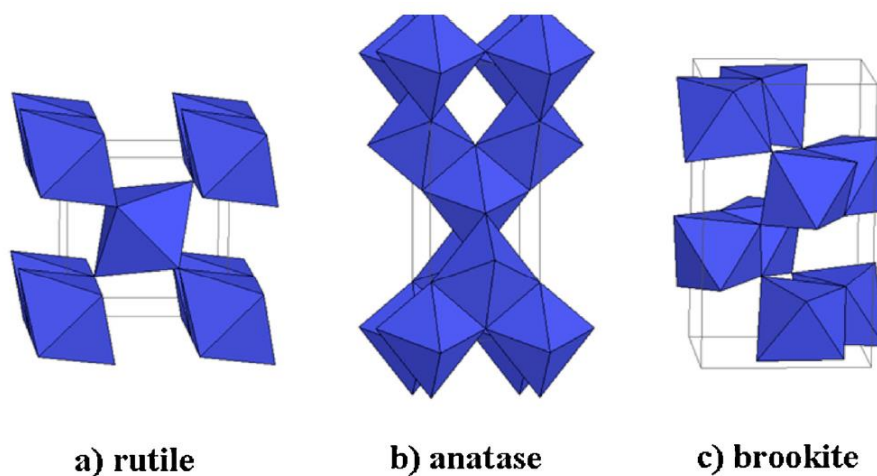


Figure 11. TiO₂ crystal structures: rutile (a), anatase (b) and brookite (c) [37]

Wu et al. (2014) observed the effect of TiO₂ calcination temperature on the photocatalytic oxidation of gaseous NH₃. Figure 12 showed the XRD patterns for TiO₂ (P25) by varying the calcination temperature. The results indicated that the phase transformation of TiO₂ was observed at 500 °C. The rutile phase of TiO₂ was commonly formed above 600 °C and completely transformed to rutile phase at 800 °C. The anatase phase was formed inherently in general TiO₂ [39].

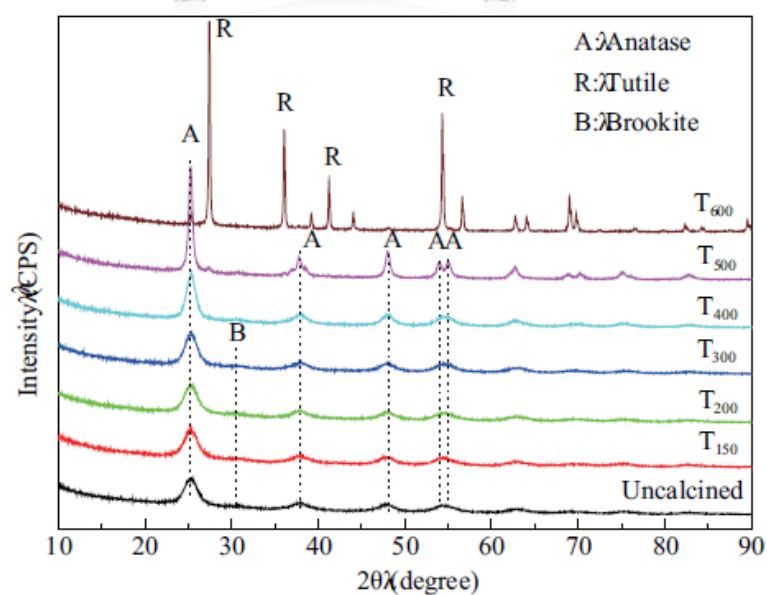


Figure 12 XRD patterns of the TiO₂ catalysts calcined at various temperatures [39]

Lu et al. (2019) studied the structure and reactivity of single site Ti catalysts for propylene epoxidation. The single-site as the 4-fold coordinated Ti site provided the high activity and selectivity of PO and improved the hydrogen efficiency on the epoxidation reaction because Ti^{4+} could be promoted $Ti\cdot OOH$. For the single-site as the 6-fold coordinated Ti site promoted the undesired byproducts such as propanal [25].

Smeets et al. (2018) focused on the cyclohexene epoxidation mechanism by using Ti-based catalysts. There were 2 pathways for Ti-based catalyst on the epoxidation reaction that occurred via the different intermediate as shown in Figure 13. The first pathway was the allylic oxidation reaction via the intermediate as $TiO\cdot$ to form the methyl ester, and then reacted with the alkene to create the oxirane ring as the epoxy product. The second pathway was the direct epoxidation reaction via the intermediate as $Ti\cdot OOH$ to form the epoxy product directly. Moreover, the large amounts of water promoted the low epoxidation activity because the water could be hydrolyzed the epoxy product to the alcohol or ketone [13].

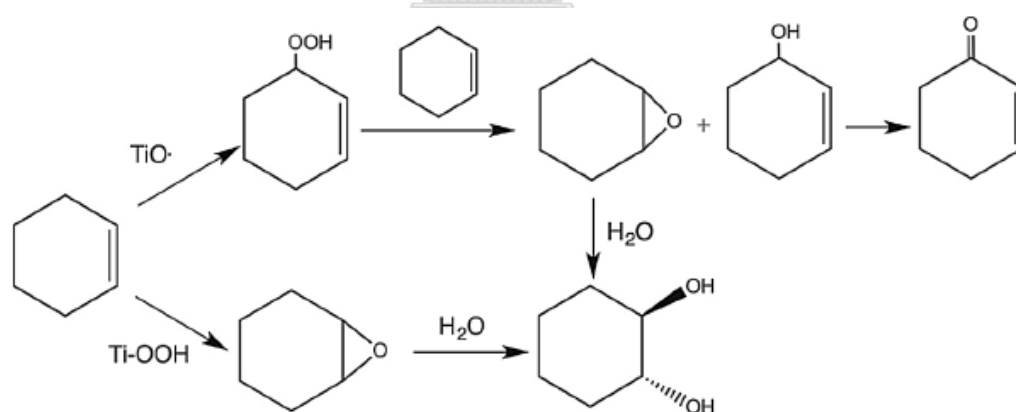


Figure 13. Reaction scheme for the epoxidation of cyclohexene via the allylic oxidation (up) or the direct epoxidation routes (bottom) [13]

Guangjian et al. (2008) studied the epoxidation of styrene with hydrogen peroxide over Mn-Ti-Al-MCM-41 molecular sieve under microwave irradiation. The reaction in the liquid phase normally occurred the metal leaching from the catalyst to the sample mixture after the reaction that confirmed by ICP-technique. Ti leaching affected the poor conversion and selectivity because the amount of active sites were decreased as the one of catalyst deactivation [21].

2.4.2 Titanosilicate (TS-1)

Titanosilicate (TS-1) is the one of popular commercial catalyst because it can provide the high catalytic activity and selectivity for partial oxidation of alkene to form the epoxy group as the desired product with hydrogen peroxide (H_2O_2). The other applications of TS-1 have the hydroxylation of aromatics, ammoximation of ketones, oxidation of alkanes and alcohols, etc. The skeletal structure (MFI) of TS-1 is the same as the ZSM-5 and It composes of the bi-directional 12-membered ring pore with the pore size along (100) as $5.1 \times 5.5 \text{ \AA}$ and $5.3 \times 5.6 \text{ \AA}$ along (010) as shown in Figure 14 and 15 [40-42].

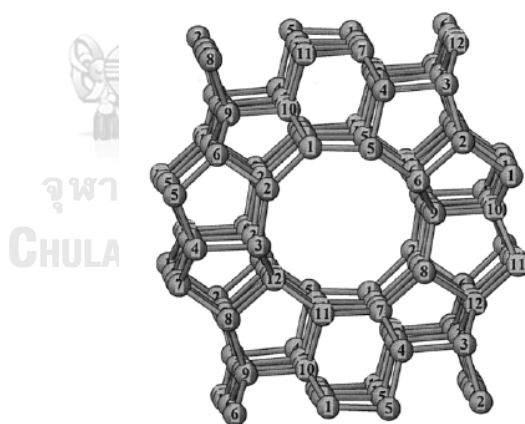


Figure 14. The structure of the orthorhombic form of silicalite (MFI-type)

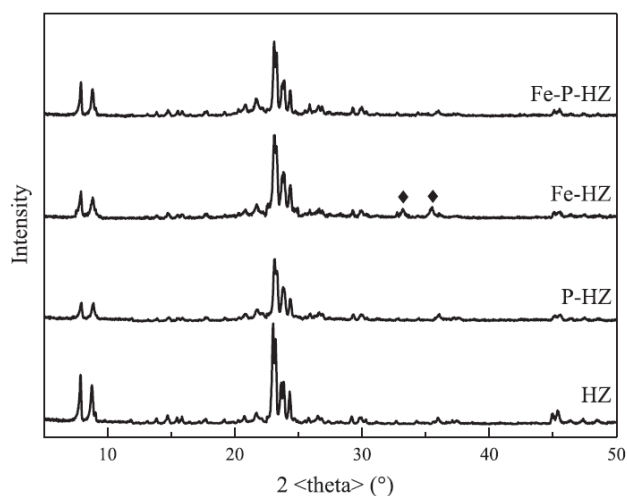


Figure 15. XRD patterns of HZ, P-HZ, Fe-HZ and Fe-P-HZ [40-42]

TS-1 is applied from the Ti-based catalyst as the crystal structure to the well-defined structure by adding the silica molecule because it can promote the Ti dispersion on the surface catalyst and increase the active site (Ti-OOH) favorably. The structure of TS-1 is the silica tetrahedral that is replaced by metal cation (such as Ti^{4+} , Fe^{3+} , or V^{3+}) in the framework positions to form like the zeolite structure [43].

Wanga et al. (2017) considered the hierarchical TS-1 synthesized via the dissolution-recrystallization process. The hydrothermal or rapid crystallization was the best method to synthesize the TS-1 framework because this method took time slightly and generated the crystal completely [44]. TS-1 was post-modified by aqueous ammonium salts and mixed with the solution of TPAOH. The results showed the pore volume of 0.22-0.28 cm^3/g and the catalytic activity in cyclohexene oxidation increased for the secondary porosity and the five- or six-coordinated extra-framework titanium species present [45, 46].

Wang et al. (2012) studied the Multilayer structured MFI-type titanasilicate including the synthesis and catalytic properties in selective epoxidation of bulky molecules. The catalytic performance of lamellar titanasilicate (LTS-1) was more active than the other Ti-based catalyst for alkene oxidation reaction with H_2O_2 . There were 3 pathways for cyclohexene epoxidation by using titanasilicate from the usability of the Ti active site. The first pathway was the isolated Ti species that catalyzed the double

bond of carbon (C=C) to form CHO. The second pathway was the radical oxidation on the allylic position to 2-cyclohexene-1-ol and 2-cyclohexene-1-one. And the final pathway was the CHO that could be hydrolyzed with water over the weak acid site in titanasilicate to form the 1,2-cyclohexanediol as the by-product [26].

Smeets et al. (2018) focused on the cyclohexene epoxidation mechanism by using Ti-based catalysts including the titanasilicate as shown in Figure 16. The tetrahedral Ti could be attacked by water and hydrolyzed one siloxane bridge. It effected the titanium coordinate changing from Ti^{4+} to Ti^{6+} , and then the coordination of water led to the formation of the activated intermediate as the hydroperoxo group (Ti-OOH). The intermediate was transferred the oxygen atom to the olefin on the direct epoxidation mechanism. The molecule of water was occurred because it was released from spent active site (Ti-OOH). The epoxy product could be hydrolyzed secondly to generate the diol-compounds which obstructed the direct epoxidation reaction [13].

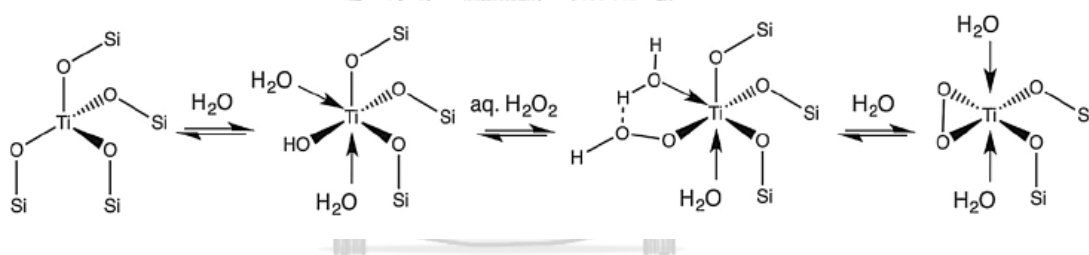


Figure 16. Mechanism of the titanasilicate epoxidation catalysts in the water [13].

2.4.3 Gamma alumina (γ - Al_2O_3)

Alumina is an important inorganic material that is widely used in many fields such as the ceramics, microelectronics, refractories, abrasives, catalysts, catalyst supports, and other fields. Alumina have the micromorphology variously to develop and determine its application by using high technology which also permits the value-added industry [47]. The performance of alumina depends on not only the particle size but also the particle shape [48].

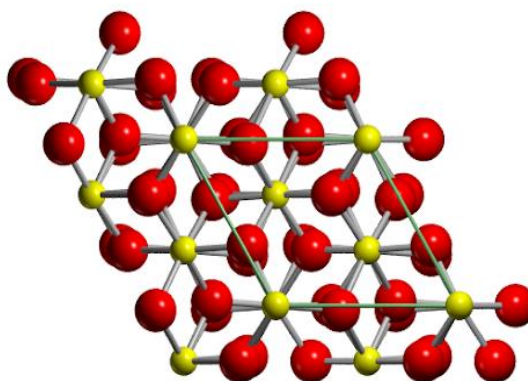


Figure 17. Gamma aluminium oxide [48]

Samadhi et al. (2016) was studied the synthesis of γ - Al_2O_3 catalyst support from kaolin of Indonesian origin. The phase transformation of alumina was an important things to specify the morphology obviously as shown in Figure 18 of only boehmite [49].

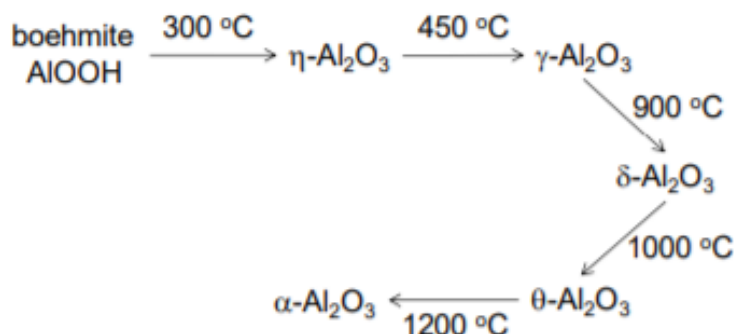


Figure 18. Boehmite dehydration and phase transition route in the Al_2O_3 system [49]

Xie et al. (2016) was observed the effect of novel synthetic methods and parameters control on morphology of nano-alumina particles. There are many crystal forms of alumina which α - Al_2O_3 and γ - Al_2O_3 were the two most common kinds to use in many fields [50]. The first one was α - Al_2O_3 which had excellent physical and chemical properties such as acidity, hardness, strength, and good heat resistance. Ceramics was required α - Al_2O_3 to produce and increase some properties. α - Al_2O_3 was observed completely at temperature of 1,200 °C [51]. The second was γ - Al_2O_3 which

also called the activated alumina. It had some good catalytic performance for chemical reaction such as large surface area, strong adsorption, and wear resistance. γ - Al_2O_3 was observed completely at temperature of 500-800°C [52]. Table 10 showed the effect of calcination temperature on the size of alumina in the presence of additives which confirmed the phase of γ - Al_2O_3 used in the research.

Table 10 Varying the calcination temperature to know the phase transformation [50]

Calcination temperature (°C)	600	800	1050	1200
Al_2O_3 crystal type	Amorphous	γ - Al_2O_3	α - Al_2O_3	α - Al_2O_3
Grain size (nm)	-	5 – 50	10 - 100	≥ 100
Color	Light yellow	White	White	White

Lu et al. (2019) investigated effects of phase transformation on properties of alumina ceramic membrane by using a new assessment based on quantitative X-ray diffraction. The results showed the characteristic peaks of other phases of alumina by heating boehmite at 450–1,300°C as shown in Figure 19 [53].

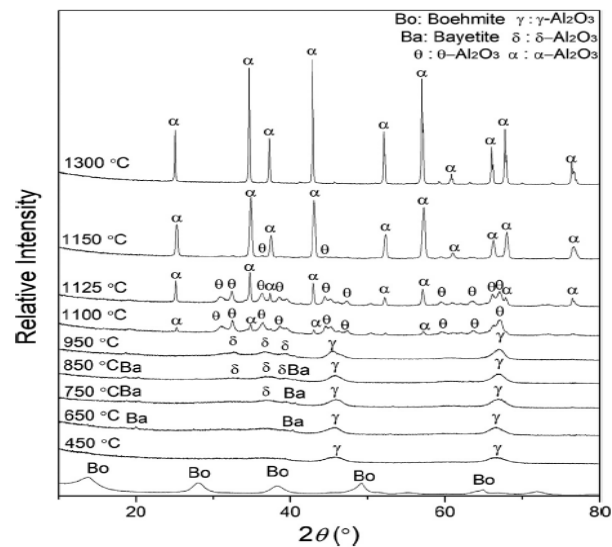


Figure 19. XRD patterns for the produced alumina membranes by heating boehmite at 450–1300°C for 0.5 h. [53]

Rinaldi et al. (2003) examined cyclohexene and cyclooctene epoxidation with aqueous hydrogen peroxide using transition metal-free sol-gel alumina as the catalyst. The results proposed the mechanism via the epoxidation by using alumina as shown in Figure 20. The hydrogen peroxide reacted with the weak acidic sites of the alumina surface to form hydroperoxo groups ($\text{Al}\cdot\text{OOH}$). The oxygen atom could be transferred to the double bond of carbon ($\text{C}=\text{C}$) by $\text{Al}\cdot\text{OOH}$ to generate the epoxy product, however $\text{Al}\cdot\text{OOH}$ also reacted with vicinal hydroxy groups (redox reaction) to form oxygen molecule and water as the by-products. The lewis acid formed in the redox reaction could regenerate the alumina surface to form the initial surface, but the effect of lewis acid promoted the ring opening reaction was more than the regeneration reaction. It might mention that the deactivation of alumina was the several rehydration step occurred until the surface changed from the original [54].

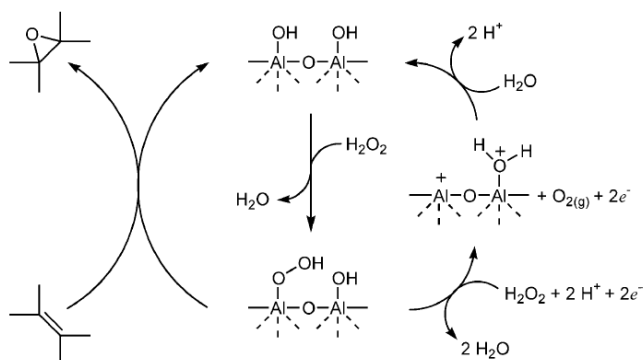


Figure 20 Proposed mechanism of the epoxidation and oxygen formation [54].

Choudhary et al. (2005) studied the epoxidation of styrene by anhydrous hydrogen peroxide over boehmite and alumina catalysts with continuous removal of the reaction water. It reported that the presence of water could block the formation of Al-OOH including the lewis acid sites of the catalyst could promote the side reaction and also block the formation of Al-OOH [55].

2.5 Deactivation of catalyst

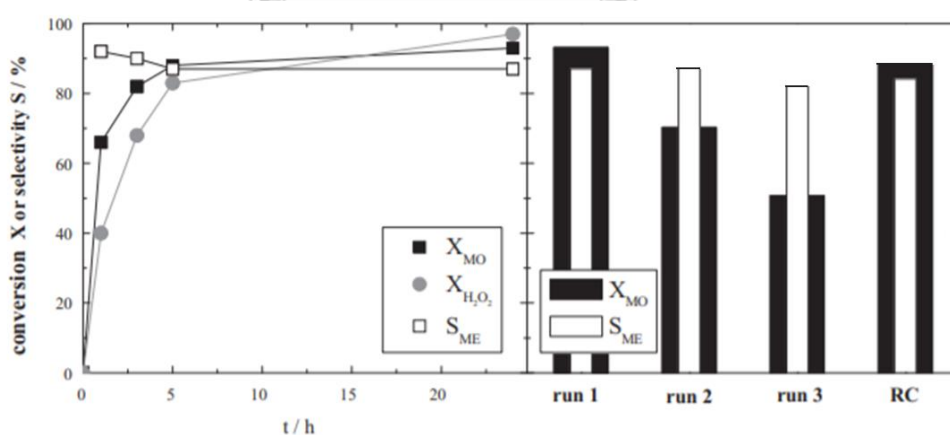


Figure 21 Catalytic activity test in the MO epoxidation over TS-1 (ind.) at 323 K (left part) and reuse or regeneration (RC: regenerated catalyst, calcination in air flow for 6 h at 823 K) of the catalyst (right part) [11].

Wilde et al. (2012) investigated on the reusability testing as shown in Figure 21. This result can prove the deactivation on the surface obviously. After the regeneration, the conversion of regenerated catalyst cannot return back to the conversion of fresh catalyst also [11].

Romero et al. (2018) investigated the epoxidation of cyclohexene over basic mixed oxides derived from hydrotalcite materials by focusing on the catalyst reutilization. It reported that the sample mixture after the reaction was carried out by filtering and washing the catalyst with the solvent, after that the solid was dried in an oven at 100 °C overnight. To determine the activation temperature of spent catalysts, they were characterized by TPO analysis [23].

Bandna et al. (2016) was reviewed that the variation in surface species viz. Ti^{3+} , Ti^{4+} , O^{2-} , oxygen vacancies, OH group and optical properties was studied by using X-ray photon spectroscopy (XPS) and UV-Vis spectroscopy. The reduction of energy gap (E_g) was directed variation with the oxygen vacancy forming due to electron transfer from semiconductor-like to a more metallic-like. The oxygen vacancy can be promoted the electron transfer to the metal site. It effected the reduction of metal site such as Ti^{4+} to Ti^{3+} , and then the electric conductivity will be increased. It affected the lower energy band due to the O_v forming [56].

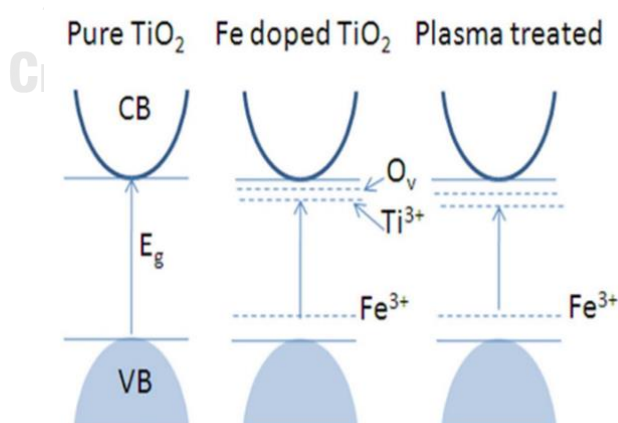


Figure 22 Schematic diagram of the energy levels of (a) pure/untreated TiO₂ films, (b) Fe doped/untreated TiO₂ film, (c) Fe doped/treated TiO₂; for 60 seconds of treatment time, (O_v represents oxygen vacancies) [56]

Ye Shui Zhang et al. (2019) investigated the formation of coke d by heavy oil volatilization/decomposition on Y-zeolite. It reported that the peak position of coke by TPO curve is comprised the peak at 80 – 100 °C as the moisture peak [57]. Additionally, the peak position of coke at 500 - 600 °C as the as the fouling on the external catalyst surface[58].

Bojan Jankovic et al. (2020) studied the assessment of spontaneous ignition potential of coals using TGA–DTG technique. Their results reveal that the peak position around 80 – 100 °C and 200 – 400 °C as the high oxygen content of fouling such as alcohol, ketone, aldehyde, and so on [59].

Ming-Lei Gou et al. (2017) studied coking and deactivation behavior of ZSM-5 during the isomerization of styrene oxide to phenylacetaldehyde. Their results reveal that the soft coke is 200 – 400 °C and the hard coke is 400 – 700 °C [60].

Ye Wan et al. (2002) studied the effect of leaching features of Fe-MCM-41 during epoxidation of alkene with hydrogen peroxide. The results provided the heterogeneous catalyst can be leached after the epoxidation reaction. Fe content remaining in the catalyst is 0.8 wt% after reaction, close to that capable of entering the framework of MCM-41 [65].

CHAPTER III

EXPERIMENTAL

This chapter concern the background knowledge and the literature review to describe the information of methyl oleate as the feedstock and methyl 9,10-epoxy stearate as the desired product. In addition, it shows the detail of epoxidation reaction and catalyst reviewing via the epoxidation reaction below.

3.1 Materials and chemicals

On the epoxidation of methyl oleate, hydrogen peroxide (H₂O₂) was used as the oxidizing reagent and acetonitrile was used as the solvent. The commercial of P25 and γ -Al₂O₃ were obtained. Naphthalene was used as the internal standard for analyzing on gas chromatography apparatus equipped with the mass spectrometric detector (GC-MS). All chemicals are shown in Table 11.

Table 11 Chemicals used in epoxidation reaction and catalyst preparation

Chemical name	Formula	Purity (%)	Suppliers
Methyl oleate	C ₁₉ H ₃₆ O ₂	99.0	Aldrich
Hydrogen peroxide	H ₂ O ₂	30 (w/w) in H ₂ O	Aldrich
Acetonitrile	CH ₃ CN	99.8	Aldrich
Naphthalene	C ₁₀ H ₈	> 98.0	Fluka
Degussa (P25)	TiO ₂	-	Aeroxide
Aluminium oxide anhydrous (Lab Grade)	γ -Al ₂ O ₃	-	Kemaus
Titanium (IV) isopropoxide (TIP)	TiOCH(CH ₃) ₂	97.0	Aldrich
Tetraethyl orthosilicate (TEOS)	Si(OC ₂ H ₅) ₄	> 99.0	Merck
Tetrapropylammonium bromide (TPABr)	C ₁₂ H ₂₈ NBr	-	Aldrich

Ammonium hydroxide	NH ₄ OH	28 (w/w) in H ₂ O	Aldrich
Isopropanol	CH ₃ CHOHCH ₃	99.0	Aldrich

3.2 Catalyst Preparation

P25 and γ -Al₂O₃ were obtained by commercial catalyst. Only TS-1 was synthesized by the hydrothermal method. The details of preparation method are presented as follows:

3.2.1 TiO₂ (P25)

Commercial titanium dioxide (TiO₂) was used as the powder catalyst. The solid catalyst should be crushed into fine powder and eliminated some impurity by filtration and washing with DI water. After that the solid solution was dried at 110 °C overnight to remove some water.

3.2.2 γ -Al₂O₃

Commercial aluminium oxide anhydrous (γ -Al₂O₃) was used as the powder catalyst. The solid catalyst should be crushed into fine powder. After that the fine powder must to eliminate some impurity and confirm the gamma alumina phase by calcination at 800 °C for 4 h under a static air atmosphere with the ramp rate 10 °C/min.

3.2.3 Titanosilicate (TS-1)

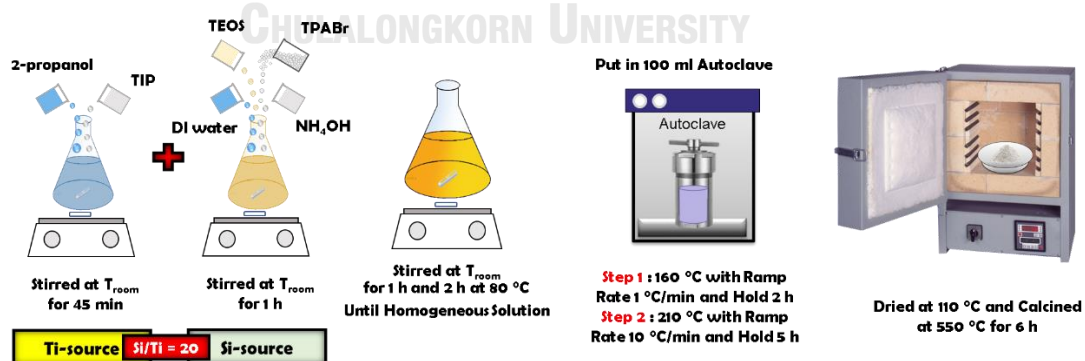


Figure 22. Synthesis of titanosilicate (TS-1) by hydrothermal method

According to Figure 23, TS-1 was synthesized by the hydrothermal method. First, titanium (IV) isopropoxide (TIP) 0.1557 g as the titanium source was added to a 100 mL beaker dissolved in isopropanol. The solution was stirred at room temperature for 45 minute until homogeneous. Second, tetraethyl orthosilicate (TEOS) 8.478 g as the silicon source, tetrapropylammonium bromide (TPABr) 2.636 g, and ammonium hydroxide 4.8438 mL (NH_4OH) were added to a 100 mL beaker dissolved in 54.8 mL distilled water. The solution was stirred at room temperature for 1 h until homogeneous. Third, the beakers were mixed and stirred first for 2 h at room temperature and, then, at 80 °C for 1 h to remove the isopropanol. Forth, the resulting solution was added to the 100 mL autoclave for crystallization. The heat step is used at 160 °C for 2 h by using ramp rate 1°C/min then, hold at 210 °C for 5 h by using ramp rate 10°C/min. Fifth, the obtained solid were washed by deionized water and centrifuged. Finally, the solid powder was dried at 110 °C for 6 h and calcined in an air atmosphere at 550 °C for 6 h to get the powder TS-1 (White powder).

3.3 Catalytic activity test on the epoxidation reaction

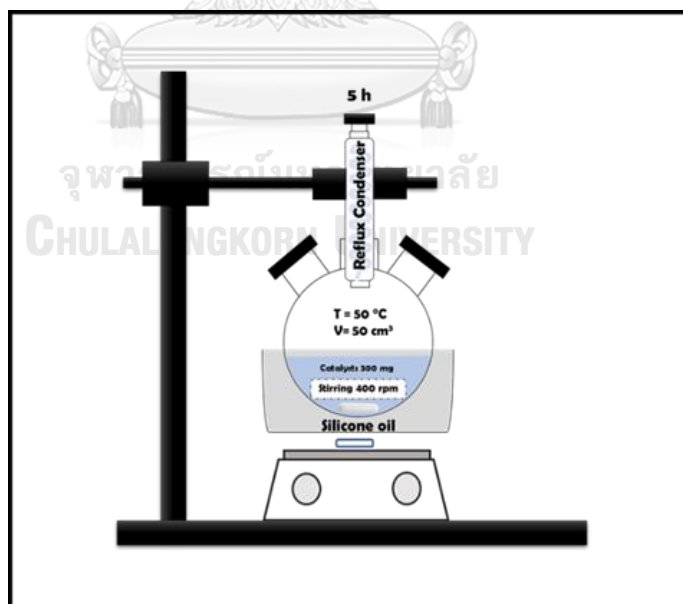


Figure 23. Epoxidation reaction of methyl oleate

According to Figure 24, the catalytic property of each catalyst was tested in a 50 cm³ three-necked round-bottom glass reactor with a reflux condenser. During the liquid-phase methyl oleate epoxidation reaction at 50 °C in oil bath, the mixture was stirred with a magnetic stirrer at 500 rpm with a reaction of 5 h. The substrates comprised (1) methyl oleate, (2) hydrogen peroxide as an oxidizing reagent and acetonitrile as the solvent. The MO/H₂O₂ feed molar ratio is 2:1, where naphthalene was used as the internal standard. The catalyst weighed 0.3 g was mixed with MO before adding H₂O₂. The liquid samples 0.2 mL were taken from the reaction mixture after 1, 2, 3, 4 and 5 h of reaction. After the reaction, the catalyst was removed by centrifugation and dried at 110 °C overnight. The spent catalysts were regenerated by calcination at 550 °C under atmospheric air for 4 h. The obtained catalysts were crushed and done the reaction again at the same condition. The activity and selectivity were calculated by both equations:

$$\text{Conversion (\%)} = \frac{\text{Moles of methyl oleate (in)} - \text{Moles of methyl oleate (out)}}{\text{Moles of methyl oleate (in)}} \times 100$$

$$\text{Selectivity (\%)} = \frac{\text{Moles of methyl oleate epoxidized}}{\text{Moles of methyl oleate (in)} - \text{Moles of methyl oleate (out)}} \times 100$$

The stability or deactivation was then examined via the percentage of lower MO conversion as shown in this equation:

$$\text{Lower MO Conversion (\%)} = \frac{\text{MO Conversion (Run 1)} - \text{MO Conversion (Run 2)}}{\text{MO Conversion (Run 1)}} \times 100$$

The liquid samples were analyzed by gas chromatography–mass spectrometry apparatus equipped with a DB–5 capillary column (30 m x 0.25 mm x 0.25 μm). All products will be promoted by the best temperature program of GC-MS. The detail of condition was shown in Figure 25

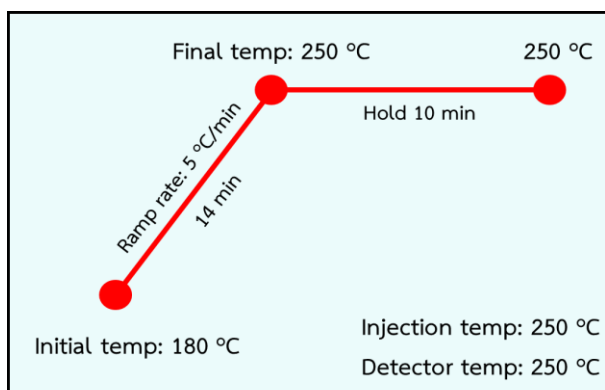


Figure 24. Temperature program of GC-MS condition

According to the Figure 25, the temperature of column was 180 °C before injection. After injection, the column was heated to 250 °C by using ramp rate 5 °C/min for 14 min. Then, held at 250 °C for 10 min.

3.4 Catalyst Characterization

The fresh catalysts and deactivated catalysts were characterized by different analytical techniques to investigate the properties of catalysts on surface and bulk including the different of properties between fresh and deactivated catalysts. There are 5 techniques as follows:

3.4.1 X-ray diffraction (XRD)

The catalysts were characterized by X-ray diffractometer Bruker D8 Advance using Cu-K α radiation between 20° to 80° for P25, γ -Al₂O₃ and 5° to 50° for TS-1, respectively. The obtained XRD patterns used with a scan speed of 0.5 sec/step. The lattice parameter and d-spacing were computed based on Bragg's law. Crystallite size was computed by Scherrer equation.

3.4.2 X-ray photoelectron spectroscopy (XPS)

X-ray photoelectron spectroscopy (XPS) was determined to investigate the oxygen vacancy (O_v) and the oxidation state of Ti, O, and Al via the binding energy measurement. The XPS spectra were obtained by AMICUS spectrometer using Mg K α X-ray radiation (1253.6 eV) and Al K α X-ray radiation (1486.6 eV) at voltage 15 kV and current of 12 mA.

3.4.3 Ultraviolet-visible spectrophotometry (UV-vis)

Ultraviolet-visible spectrophotometry (UV-vis) was examined to investigate the energy gap by the adsorption versus energy profiles and confirm the oxygen vacancy (O_V) including the detail of coordination geometry of Ti cations and the ligand environment. The curves was used in range of 200 – 500 nm obtained by Perkin Elmer Lambda 650 spectrophotometer. The step size for the scan was 1 nm.

3.4.4 Temperature programmed oxidation (TPO)

The amount of carbon content in the catalyst was determined by TA Instruments SDT Q 600 analyzer, which measures the amount of weight changed of material after reaction testing and provided the chemical phenomena such as decomposition temperature (finding reaction temperature range), and solid-gas reactions (oxidation). The samples of 10-20 mg and a temperature ramping from 298 to 1273 K at 2 K/min were used in the operation with N_2 UHP carrier gas.

3.4.5 Fourier-transform infrared spectroscopy (FT-IR)

FT-IR analysis was used to provide functional group as a chemical structure of the catalyst. FT-IR was obtained by using a Nicolet 6700 FT-IR spectrometer. Catalyst was performed on compacted powder disk of 0.5-1 g of each catalyst.

3.4.6 Inductively coupled plasma - optical emission spectrometry (ICP-OES)

ICP-OES analysis was tested to suggest the leaching effect of Ti and Al metal sites from the catalyst after the reaction. ICP-OES was obtained by using a 2100 DV from Perkin Elmer. The liquid sample was diluted by DI water before measuring the metal site in the solution.

CHAPTER IV

RESULTS AND DISCUSSION

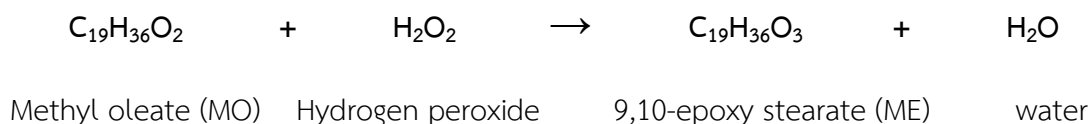
The results and discussion in this chapter are divided into three parts. The first part concerned the deactivation of P25, TS-1 as the Ti-based catalysts, and γ -Al₂O₃ during the methyl oleate (MO) epoxidation to indicate the deactivation effects on the surface confirmed by XPS, UV-vis, TPO, FTIR, and ICP-OES techniques. The second part investigated the regeneration part that the effect of calcination temperature (550 °C, 700 °C) were varied to find out the optimum condition which eliminated the fouling effects completely confirmed XRD techniques. In addition, the analysis on the regeneration of TS-1 surface was concerned to clarify the lower MO conversion that could not return back to the MO conversion of fresh TS-1 catalyst.

4.1. Deactivation of P25, TS-1, γ -Al₂O₃ during the MO Epoxidation

To understand the deactivation on the P25, TS-1 as the Ti-based catalysts, and γ -Al₂O₃ as the Al-based catalyst during MO epoxidation. The reusability testing was concerned by investigating the lower MO conversion as the deactivation rate after multiple reuses.

4.1.1. Investigation the deactivation rate on the P25, TS-1, γ -Al₂O₃

The epoxidation of methyl oleate (MO) to methyl 9,10-epoxy stearate (ME) was carried out in liquid-phase reaction with hydrogen peroxide (H₂O₂) at 50 °C and 1 atm. The reaction was exhibited in the equation below:



After multiple reuses, the percentage of lower MO conversion was investigated to verify the catalyst that were deactivated faster than the others shown in Figure 26.

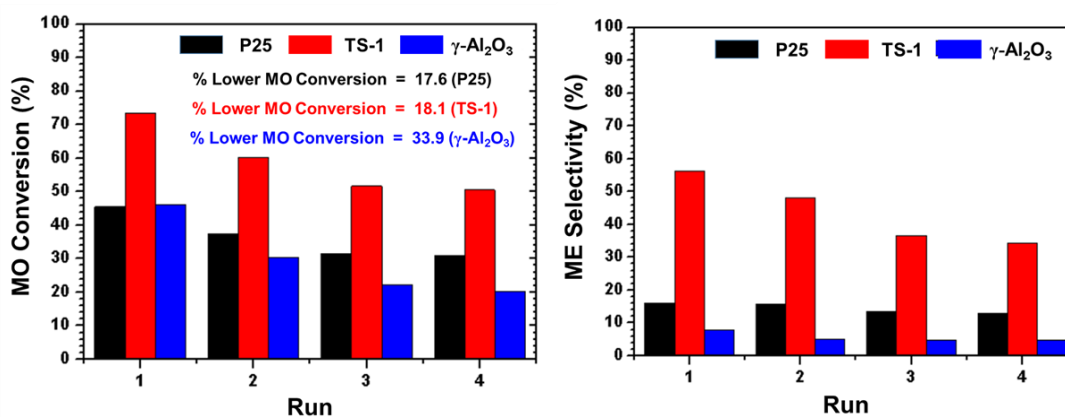


Figure 25. The reusability testing in a 50 cm³ three-necked round-bottom glass reactor during MO epoxidation with H₂O₂ over difference catalysts at 50 °C for 5 h.

In the 1st run of MO epoxidation reaction, the TS-1 gives the highest MO conversion with 73.5%. And the γ -Al₂O₃ gives the lowest MO conversion with 46.2%. This result reveals that TS-1 is high performance catalyst for MO epoxidation corresponding to the Smeets et al. works [13]. However the conversion of synthesis TS-1 is not equal to the conversion of TS-1 similarly with the P25 and γ -Al₂O₃ because the used condition is not the best condition for TS-1 and γ -Al₂O₃ but the researcher need to control the independent variable effectively such as the concentration of H₂O₂ and time. This condition is suitable for only TiO₂ [13]. Furthermore, the percentage of lower MO conversion was observed to compare the stability of these catalysts. The percentage of lower MO are approximately 17.6, 18.1, and 33.9 for P25, TS-1, and γ -Al₂O₃ respectively. The deactivation is occurring when these catalysts are reused. The MO conversion of γ -Al₂O₃ fell significantly with a higher rate than the P25 and TS-1. Not only γ -Al₂O₃ gives the lowest MO conversion and ME selectivity, but also give the lowest stability in term of deactivation compared with P25 and TS-1. In part of ME selectivity, the γ -Al₂O₃ gives the lowest ME selectivity because it produces more by-products such as methyl 9,10-epoxy stearate, methyl 9,10-dihydroxy stearate, methyl keto stearate(1&2), nonylaldehyde, and methyl 9-oxononanoate corresponding to Turco et al. (2016) works [14]. This reason may be affected the highest deactivation rate on γ -Al₂O₃.

To explain the deactivation rate of these catalysts, the crystallinity were concerned to describe the characteristic of catalyst and find out why the γ -Al₂O₃ gives the lowest stability. Because the γ -Al₂O₃ shows the amorphous structure as the lowest crystallinity compared with P25 and TS-1 according to the Table 12. For γ -Al₂O₃ catalyst, the crystallinity do not affect the deactivation rate when it compare with the P25 and TS-1. It may have some effects that cause the deactivation. However, this study does not clear to justify the relationship between crystallinity and stability. Thus, it must study to the next time.

Table 12 Crystallite size and the crystallinity of fresh catalysts

Catalyst	Crystallite size (nm)	Crystallinity (%)
P25	20.8	41.9
TS-1	24.5	65.2

To justify the lower MO conversion, we hypothesize that there are 2 deactivation effects on the surface catalyst. The first effect is the fouling effect that confirms by TGA and TPO techniques. The second effect is the loss of active species as the oxygen vacancy changing on the surface catalysts that confirms by XPS and the leaching effect that confirms by ICP-OES technique.

In addition, the homogeneous catalysts were also test in the MO epoxidation to compare with the heterogeneous reaction. The results show that the conversion from the H₂SO₄ catalyst is around 93.6%. The low selectivity is found of 5.1 % that is the main problem for homogeneous reaction because the reactant as the methyl oleate are cracked to the low molecules. The results is not correlated with the small molecule alkene epoxidation[61]. Hence, it should be studied deeply to the next time to solve this problem.

4.1.2. The fouling deposits on the P25, TS-1, and γ -Al₂O₃ surfaces

The fouling effect was investigated on the P25, TS-1, and γ -Al₂O₃ surfaces because these catalyst can be produced many by-products such as methyl 9,10-epoxy stearate, methyl 9,10-dihydroxy stearate, methyl keto stearate(1&2), nonylaldehyde, and methyl 9-oxononanoate proposed on the ME selectivity [14]. TGA and TPO techniques were necessary examined to describe the lower their MO conversion as shown in Figure 27 and Figure 28. The weight loss of these catalysts after the reaction is approximately 94.7% for P25, 96.2% for TS-1, and 92.4% for γ -Al₂O₃. The weight loss between 120–200 °C is caused by the volatile moisture content [57]. And the weight loss between 200–600 °C is caused by the epoxidation reaction.

It illustrates that all catalyst have the fouling deposit on the surface after the reaction. γ -Al₂O₃ shows the highest percentage of weight loss compared with the P25 and TS-1. It seems that the γ -Al₂O₃ is more deactivated than P25 and TS-1 and the fouling deposits are different on the other catalysts. As this reason, the fouling on the γ -Al₂O₃ may be (1) more than other surfaces or (2) strong adsorption than other surfaces. Thus, the types of fouling deposits were observed by TPO plot, where the used catalysts after finished the 1st run are considered.

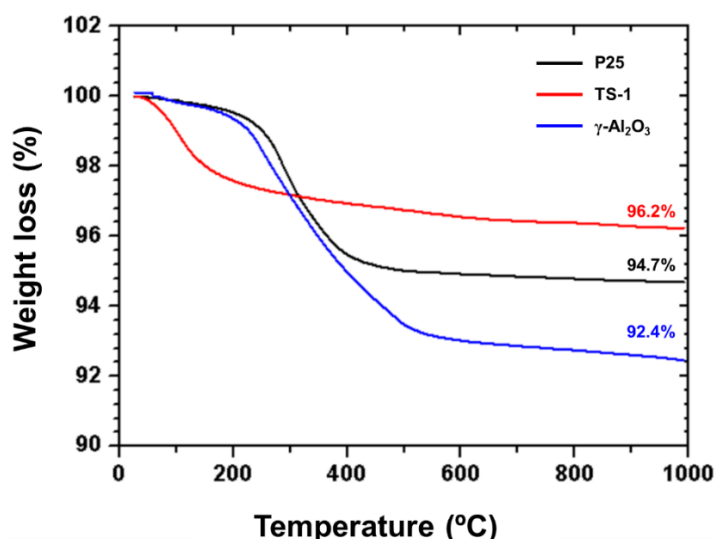


Figure 26 Thermal gravimetric analysis (TGA) of used P25, TS-1, and γ -Al₂O₃ catalysts

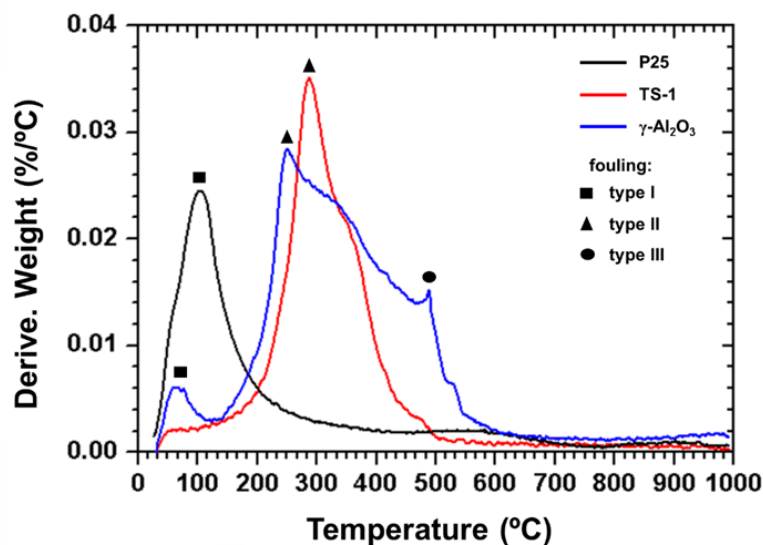


Figure 27. Temperature program oxidation (TPO) plots of used P25, TS-1, and γ -Al₂O₃ catalysts

According to the Figure 28, there are three types of fouling deposits, where type1 is found at 80 – 100 °C as the moisture peak [57], type2 is appeared at 240 – 320 °C as the soft fouling, and type3 is revealed at 500-550 °C as the fouling on the external catalyst surface including hard fouling [62], respectively. It is important to describe that the difference in the fouling behavior of the catalyst should be mainly caused by the difference active phase corresponding to Ordóñez et al. works [63]. Type1 and type2 are found in only P25 and TS-1, accordingly, while the γ -Al₂O₃ can be found three types. To expand this concern, we investigate the functional group of the fouling through FT-IR technique, where the used catalysts after finished the 1st run are considered. As the TPO results, we consider the functional group using the FT-IR profiles illustrated in Figure 29, in which the fresh and 1st run catalysts are compared. For the P25 that we find only type1, Figure 29(a2) shows two peaks changed in the 1st run; one is appeared at 1550 cm⁻¹ indicating an alkane group as a C–H bonding and the others is observed at 1420 cm⁻¹ denoting an alcohol group as O–H bonding. Also, three peaks are occurring in the TS-1 as Figure 29(b2), in which these peaks arise at 1612 cm⁻¹ representing an α,β -unsaturated ketone group as C=O bonding and at 1510 cm⁻¹ and 1455 cm⁻¹ signifying the alkane group as C–H bonding. Besides, we find three peaks for the γ -Al₂O₃ illustrated in Figure 29(c2), where the stretching ester group

as C=O bonding is found at 1736 cm^{-1} and the alkane group as C-H bonding is observed at 1594 cm^{-1} and 1421 cm^{-1} . From the TPO curve, the fouling type 2 is dominated on the deactivation effect on the TS-1 and $\gamma\text{-Al}_2\text{O}_3$ and the fouling type 1 is dominated on P25 only. Although the selectivity problem affect for the analysis in quantitative fouling formation, but the peak position and the types of fouling deposits are not changed.

To confirm the functional group of fouling deposits, the spent catalyst was diluted with the solvent and analyzed with GC-MS, It found that the P25, TS-1, and $\gamma\text{-Al}_2\text{O}_3$ was found the alcohol, ketone, and ester groups respectively. Obviously, the main deactivation of epoxidation is the fouling because the MO conversion increased after the calcination at $550\text{ }^\circ\text{C}$ and $700\text{ }^\circ\text{C}$.

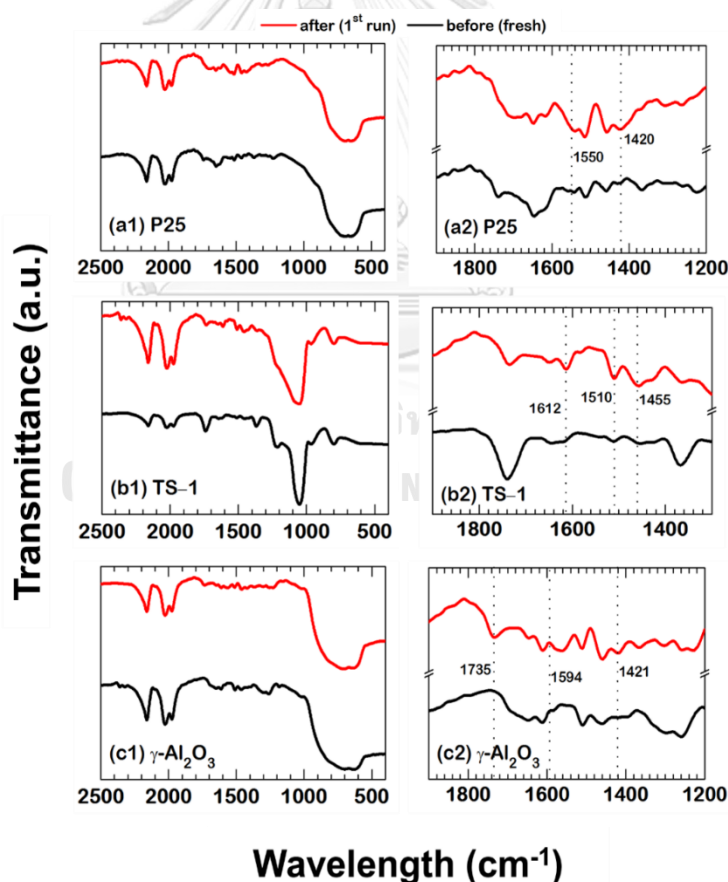


Figure 28. Fourier transform infrared spectroscopy (FT-IR) of before (a1) and after (a2) reaction of P25, TS-1, and $\gamma\text{-Al}_2\text{O}_3$ catalysts

4.1.3. The oxygen vacancy on the surface

To produce the methyl epoxy product (ME), the oxygen molecules form hydrogen peroxide were added in the catalyst surface to promote Ti-OOH as the active site. Ti-OOH groups can add the oxygen molecule to the C=C bond in the methyl oleate (MO) molecule to generate the desired product. It effects some oxygen molecule leaving out from the surface catalyst. Thus, the oxygen vacancy may occur and perform the defects on the surface of catalyst after the epoxidation reaction [56]. It effects to loss of active site also. To study the change of Ti and O state including the oxygen vacancy, the X-ray photoelectron spectroscopy (XPS) technique was analyzed. The high resolution XPS spectra profiles of P25 and TS-1 are shown in Figures 30 and 31, where the amount of Ti state and O vacancy is examined in Table 13. According to Figure 30, the XPS spectra of P25 and TS-1 showed the $Ti^{4+}2p_{3/2}$ at binding energy 458.6 and 464.2 eV are in good agreement with the TiO_2 lattice [64]. $Ti^{3+}2p_{1/2}$ was found at binding energy 460.2 eV for P25 and TS-1. After the reaction, the percentage of Ti^{3+} increased and the percentage of Ti^{4+} decreased which Ti state was changed from Ti^{4+} to Ti^{3+} that appeared in both P25 and TS-1 catalysts. Decreased Ti^{4+} showed the loss of active site on the surface which caused the lower MO conversion after the reaction. In the fresh catalysts, the $Ti^{3+}2p_{1/2}$ was faced between the small and high peaks of the $Ti^{4+}2p_{3/2}$ which implied to Ti_2O_3 phases appearance on the fresh P25, but it's not found in the fresh TS-1 [56]. The $Ti^{3+}2p_{1/2}$ peak of fresh TS-1 is around 8.3% which has less than the $Ti^{3+}2p_{1/2}$ peak of fresh P25 (13.3%). In the deactivated catalyst, the results indicate that $Ti^{3+}2p_{1/2}$ increase when these catalysts reused. The TS-1's $Ti^{3+}2p_{1/2}$ increase to 18.9% more than the P25's that increase from 13.3% to 14.2%. Moreover, the oxygen vacancy site (O_V) was examined through the XPS technique. The high resolution XPS spectra profile of oxygen is included lattice oxygen (O_L), sub oxide (O_S), and oxygen vacancy (O_V) as shown in Figure 31. The result reveals that the oxygen vacancy site (O_V) was observed only deactivated P25 (20.6%) and TS-1 (21.2%) catalysts. Therefore, TS-1 is more deactivated than P25 due to higher O_V occurrence. By the way, the observed O_L , O_S , and O_V are in good agreement with the previous work of Bharti et al [64]. The O_V observed in the deactivated catalysts confirmed that the MO epoxidation reaction remove that oxygen in the active site.

Table 13 XPS data of different oxidation state of Ti and O on the surface of TiO₂ (P25) and titanosilicate (TS-1) where O_L represents the lattice oxygen, O_S represents the sub oxide, and O_V represents the oxygen vacancies.

State		Fresh P25	Deactivated P25	Fresh TS-1	Deactivated TS-1
Ti ⁴⁺ (unit area)	Ti2p 3/2	18,686.4	7,307.5	3,557.4	3,163.2
	Ti2p 1/2	-	-	-	-
Total percentage of Ti ⁴⁺		86.7	85.9	91.7	81.1
Ti ³⁺ (unit area)	Ti2p 3/2	-	-	-	-
	Ti2p 1/2	2,865.2	1,206.7	321.6	1,210.0
Total percentage of Ti ³⁺		13.3	14.2	8.3	18.9
O (unit area)	O _L	13,214.5	4,770.2	5,397.5	1,140.0
	O _S	12,103.1	7,719.4	55,759.8	17,755.0
	O _V	-	3,239.2	-	5,093.9
Total percentage of O _V		-	20.6	-	21.2

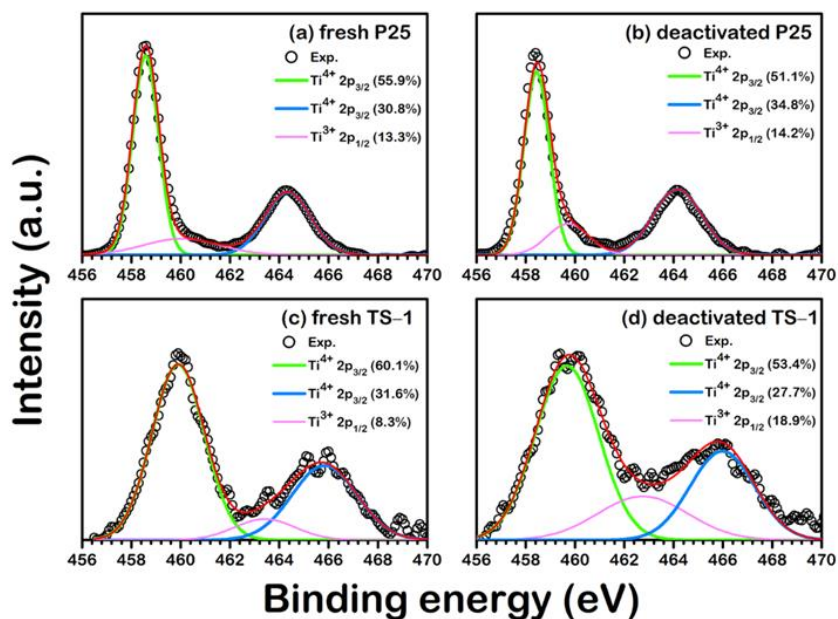


Figure 29 The high resolution XPS spectra of Ti2p in the fresh and deactivated of (a, b) P25 and (c, d) TS-1 Ti-based catalysts.

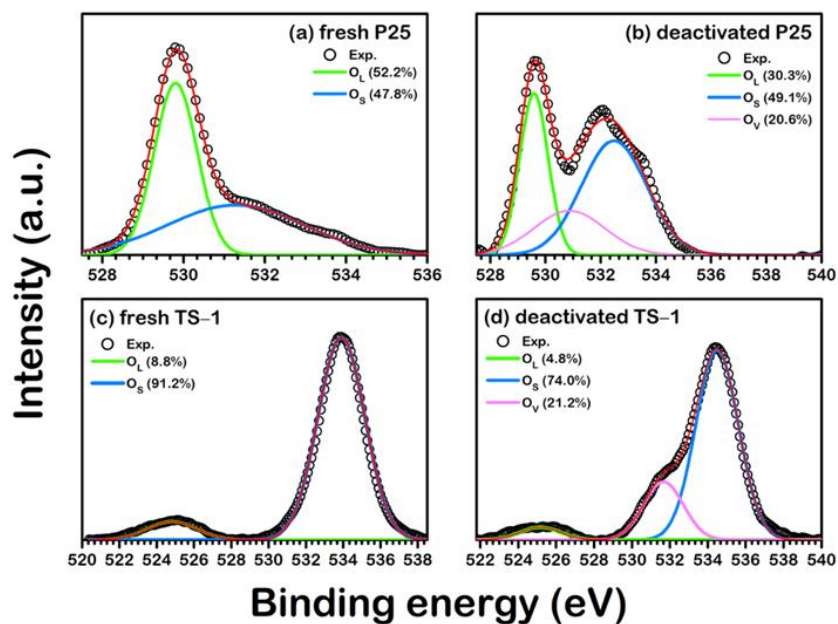


Figure 30 The high resolution XPS spectra of O1s in the fresh and deactivated of (a, b) P25 and (c, d) TS-1 Ti-based catalysts

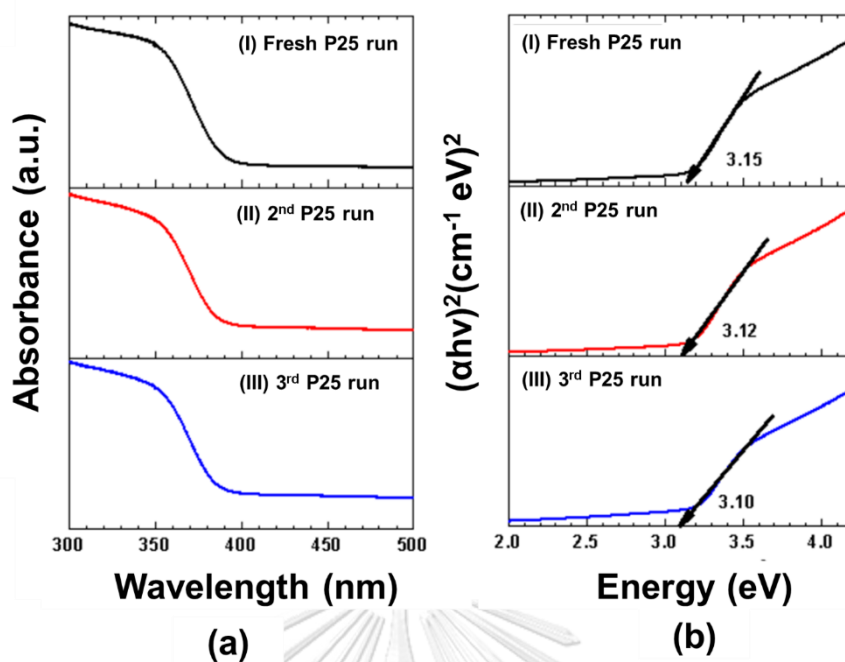


Figure 31 (a) UV spectroscopy profile of (I) fresh P25, (II) 2nd run of P25, and (III) 3rd run of P25 catalysts (b) TUAC relation plot of (I) fresh P25, (II) 2nd run of P25, and (III) 3rd run of P25 catalysts

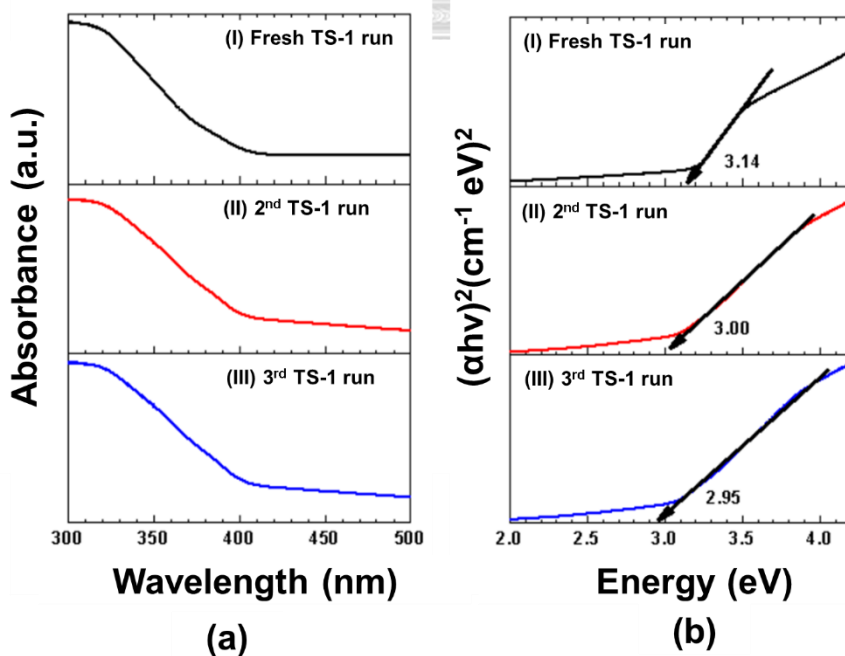


Figure 32. (a) UV spectroscopy profile of (I) fresh TS-1, (II) 2nd run of TS-1, and (III) 3rd run of TS-1 catalysts (b) TUAC relation plot of (I) fresh TS-1, (II) 2nd run of TS-1, and (III) 3rd run of TS-1 catalysts

To confirm the oxygen vacancy site (O_v), the energy band gap was concerned by UV-vis technique because O_v forming affected the lower energy gap (E_g) [65]. The reduction in energy gap might cause surface characteristic changing from semiconductor-like to a more metallic-like. The oxygen atoms were lost until it formed the oxygen vacancy site. So, the lower (E_g) affects the activity of these surfaces [58]. Figure 32 and Figure 33 reveal that the E_g decreased from 3.15 to 3.12 eV for P25 and from 3.00 to 2.70 eV for TS-1 due to the catalyst deactivation after they underwent the MO epoxidation. It observed that the rate of decreasing E_g of TS-1 is higher than P25. Consequently, TS-1 is more deactivated than the P25 because O_v forming on the TS-1 surface more than P25 surface catalyst.

The oxygen vacancy is confirmed and occurred after the epoxidation reaction obviously, but it not have evidence to indicate the cause of the loss of active spices as the oxygen vacancy forming because the active site (X-OOH) cannot characterize directly. Consequently, it should be studied deeply to the next time for confirming the loss of active spices.

4.1.4. The leaching effect

The leaching effect was examined to clarify the loss of active spices from the liquid sample after running the reaction for 5 h. Then, the samples were diluted by the DI water to measure the ICP-OES effectively. The composition of metal sites in the liquid sample is shown in Table 14. The concentration of Ti is observed approximately 8.0 $\mu\text{g/L}$ for P25 and 2.0 $\mu\text{g/L}$ for TS-1. This result reveals that the P25 give the higher leaching effect than the TS-1 because the particle size and crystallite size of P25 is lower than TS-1. For $\gamma\text{-Al}_2\text{O}_3$, the concentration of Al is found around 5.0 $\mu\text{g/L}$. Obviously, All catalyst in this work have the leaching effect after running the reaction because the epoxidation occurs in the liquid phase corresponding to Chenglong Liu works [66]. Its work review that the Ti and Fe can be leached around 7-10 $\mu\text{g/L}$. However, the leaching effect may not affect the deactivation of the P25, TS-1, and $\gamma\text{-Al}_2\text{O}_3$ because it may occur the error form the centrifugation step which the liquid sample still remain the catalyst due to transparent solution.

Table 14 Concentration of metal oxide in the liquid samples by ICP-OES measurement

Catalyst	Concentration of Ti or Al ($\mu\text{g/L}$)
P25	8.0
TS-1	2.0
$\gamma\text{-Al}_2\text{O}_3$	5.0

4.2. Regeneration of P25, TS-1, $\gamma\text{-Al}_2\text{O}_3$ after the MO Epoxidation

The previous part is talking the deactivation on P25, TS-1, and $\gamma\text{-Al}_2\text{O}_3$ during the MO epoxidation. The fouling deposit is the main effect that causes the catalyst deactivation after the reaction. So, the calcination as the regeneration method will be concerned to eliminate some fouling on the surface.

4.2.1. Investigation the catalytic activity after the regeneration

All catalysts were regenerated after the regeneration by calcination at 550 °C and 700 °C for 6 h from TPO-results. According to Figure 34, P25 and TS-1 calcined at 550 °C can be improved the 2nd conversion. Meanwhile, for Al-based catalyst, $\gamma\text{-Al}_2\text{O}_3$ not yields the conversion closed to the 1st run. It means that the fouling deposit on the $\gamma\text{-Al}_2\text{O}_3$ is not eliminated completely. Obviously, the MO conversion could not return back to the MO conversion of fresh P25, TS-1, and $\gamma\text{-Al}_2\text{O}_3$ when the catalyst calcined at 550 °C because the surface catalyst may remain some fouling deposit or O_v defects after the calcination. For P25 and TS-1 calcined at 700 °C, the MO conversion can be improved the 2nd conversion form the P25 and TS-1 calcined at 550 °C. For $\gamma\text{-Al}_2\text{O}_3$ calcined at 700 °C, the fouling on $\gamma\text{-Al}_2\text{O}_3$ can be eliminated leading to increase the conversion. P25 and TS-1 may require the calcination temperature less than 550 °C which is enough to reboot the conversion of Ti-based catalysts. $\gamma\text{-Al}_2\text{O}_3$ gives the highest percentage of lower MO conversion compared with the P25 and TS-1 because the fouling deposit on $\gamma\text{-Al}_2\text{O}_3$ is stronger adsorption than the fouling deposit on P25 and TS-1. Additionally, the fouling effect is the main deactivation during the MO epoxidation on P25, TS-1, and $\gamma\text{-Al}_2\text{O}_3$.

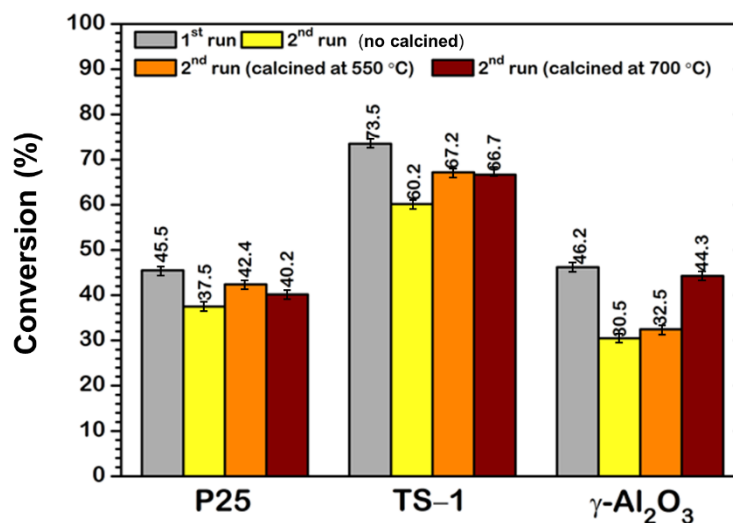


Figure 33. The MO conversion of P25, TS-1, and γ -Al₂O₃ catalysts through the MO epoxidation reaction with variation of calcination temperature

4.2.2. The effect of phase structure and crystallinity of catalyst

XRD patterns of P25, TS-1, and γ -Al₂O₃ were shown in Figure 35 – 37 including the crystallite size and crystallinity are shown in Table 15. This result reveals that the phase structure of P25, TS-1, and γ -Al₂O₃ do not change after the calcination at 550 °C and 700 °C. Therefore, the phase changing after the calcination does not cause the deactivation effect on the surface catalyst to reduce the MO conversion. However, the crystallite size and crystallinity decreased after the calcination. It may be indicated that once the catalysts are calcined, its loss the stability performance in the next time.

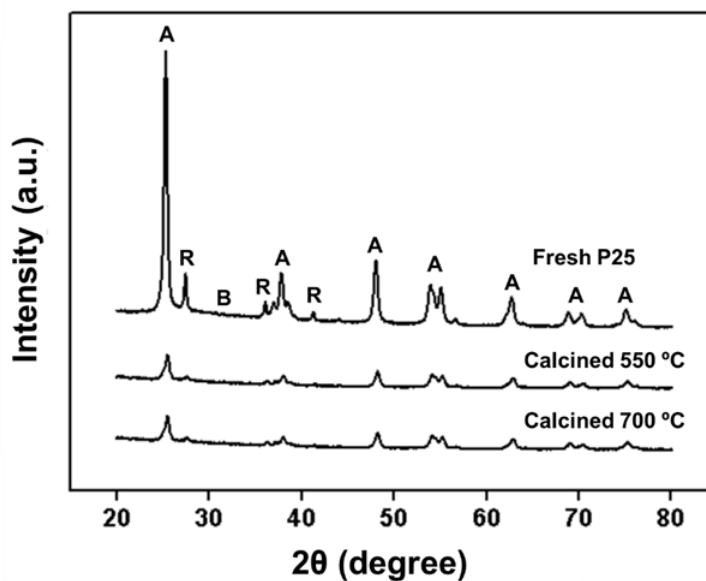


Figure 34. XRD patterns of fresh P25 and regenerated P25 with difference calcination temperature (550 °C and 700 °C)

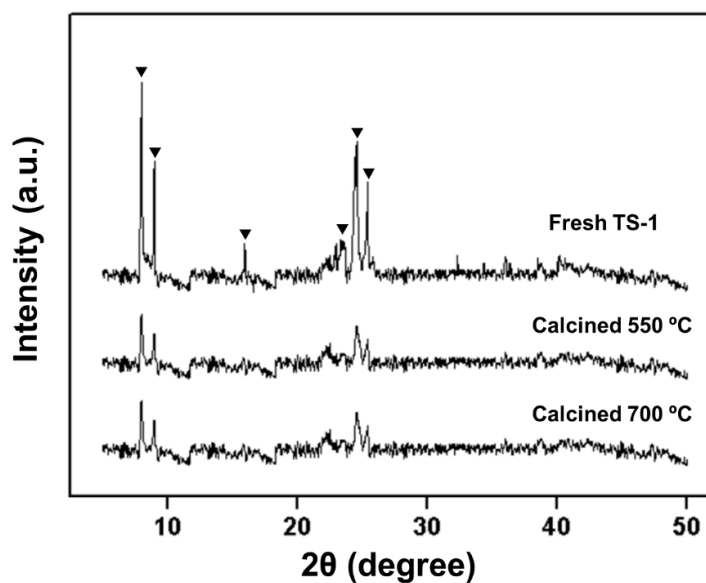


Figure 35. XRD patterns of fresh TS-1 and regenerated TS-1 with difference calcination temperature (550 °C and 700 °C)

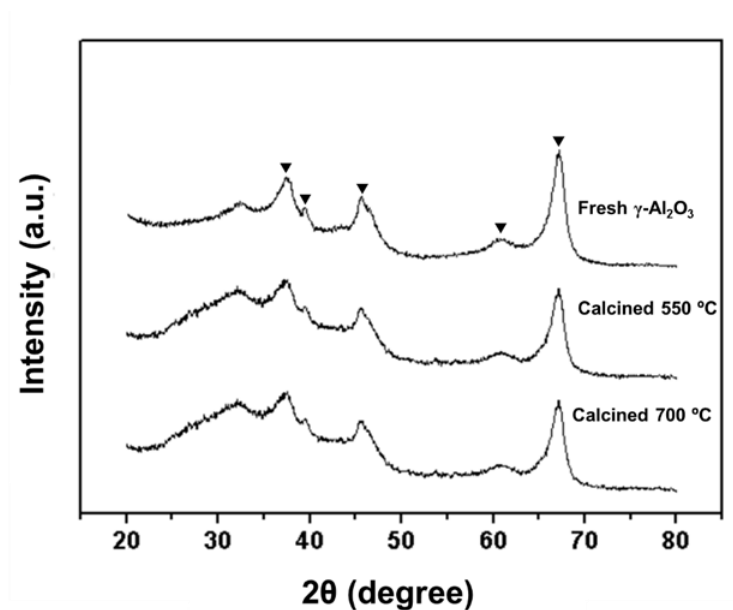


Figure 36. XRD patterns of fresh γ -Al₂O₃ and regenerated γ -Al₂O₃ with difference calcination temperature (550 °C and 700 °C)

Table 15 Crystallite size and the crystallinity of P25 and TS-1 catalysts after the regeneration at 550 °C and 700 °C calculated by Scherrer equation

Catalyst	Crystallite size (nm)	Crystallinity (%)
Fresh P25	20.8	41.9
Calcined 550 °C	5.83	30.8
Calcined 700 °C	5.32	29.5
Fresh TS-1	24.5	65.2
Calcined 550 °C	12.6	50.5
Calcined 700 °C	11.2	48.7

After the regeneration, the catalytic conversion of regenerated TS-1 cannot return back to the conversion of fresh catalyst. To find out this reason and improve the stability of TS-1, the surface properties of regenerated TS-1 will be investigated.

4.2.3. Analysis on the regeneration of TS-1 surface

The catalytic conversion of MO was analyzed to understand the deactivation mechanism and improve the stability of TS-1 including the regeneration as well. The MO conversion and ME selectivity were shown in Figure 38. These results show that the MO conversion of fresh, spent, and regenerated TS-1 catalysts are 73.5%, 60.2%, and 67.2% respectively. Obviously, the MO conversion and ME selectivity decreases after running the reaction. Although the regeneration can build up the performance of TS-1, but the MO conversion cannot return back to the conversion of fresh catalyst at 73.5%. Thus, the deactivation still remain on the TS-1 surface after the regeneration certainly. First, we investigate the fouling effect on the surface by TPO profile.

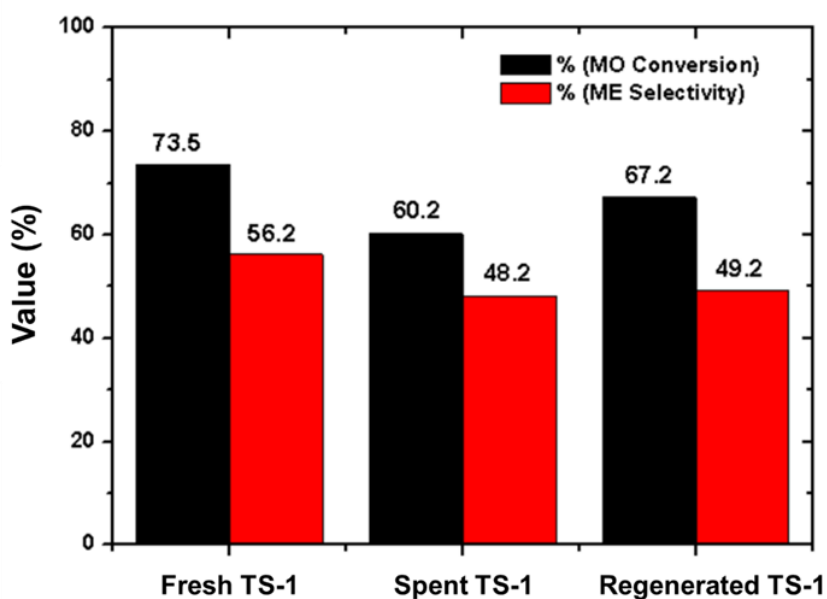


Figure 37. The MO conversion and ME selectivity of fresh TS-1, spent TS-1, and regenerated TS-1 catalysts at 550 °C via MO epoxidation in a 50 cm³ batch reactor at 50 °C

To describe the surface properties after the regeneration, many techniques were examined as TPO, XPS, and UV-vis techniques. Firstly, the TPO profile was examined to verify the deactivation on the TS-1 surface as shown in Figure 39. The fouling effect was found at 280 °C after the reaction that caused the deactivation of TS-1. However, the fouling deposits were eliminated totally by calcination at 550 °C that confirmed by the TPO profile of regenerated TS-1. Even so, the catalytic conversion of regenerated TS-1 cannot return back to the conversion of fresh catalyst. The TS-1 surface have some defects after the reaction. In this way, we investigate the surface properties of TS-1 catalyst to find the defects on the surface after the regeneration.

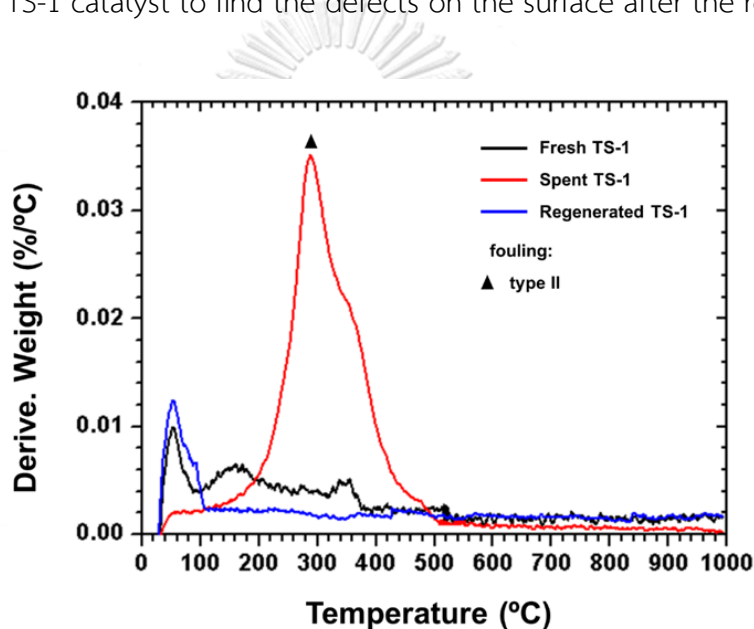


Figure 38. Temperature program oxidation profile of fresh TS-1, spent TS-1, and regenerated TS-1 catalysts

Secondly, The X-ray photoelectron spectroscopy (XPS) technique was analyzed to explain the Ti2p and O1s state on the surface. These results were shown in Figure 40 and Figure 41. The Ti2p peaks comprised (1) Ti^{4+} $2p_{3/2}$ at binding energy 458.6 eV and 464.2 eV and (2) Ti^{3+} $2p_{1/2}$ at binding energy 463.2 eV which correspond with the high resolution XPS spectra of the commercial TS-1 catalyst resulting the good agreement with TiO_2 lattice [64]. From the fresh TS-1 catalyst, TiO_2 with tetrahedral coordinate (Ti^{4+}) as the active site for MO epoxidation was found approximately 91.7% corresponding to give the high performance for TS-1. Also, Ti^{3+} was found

approximately 8.3% as shown in Figure 40(a). Nevertheless, the percentage of Ti^{4+} decreased to 81.1% that came from the deactivation effect and the percentage of Ti^{3+} increased to 18.9% after the MO epoxidation as shown in Figure 40(b). The Ti^{4+} and Ti^{3+} peaks were recovered by the calcination at 550 °C which built up to 81.7% for Ti^{4+} and 18.3% for Ti^{3+} , respectively as shown in Figure 40(c). By the way, the oxygen vacancy was investigated on the O1s XPS spectra in Figure 41. The O1s peaks comprised (1) lattice oxygen (O_L) at binding energy 525 eV, (2) sub oxide (O_S) at binding energy 534.4 eV, and (3) oxygen vacancy (O_V) at binding energy 531.2 eV. The percentage of O_V was found approximately 21.2% after the reaction. The observed O_L , O_S , and O_V are in good agreement with Bharti et al. work [64]. These results reveal that the O_V still exist around 14.6% after the regeneration. O_V forming displayed the deactivated catalyst as the defects on the TS-1 surface. Furthermore, O_V is confirmed that the MO epoxidation reaction removes that oxygen in the active site. The O_V behavior can be ensured by the energy gap analysis.

Thirdly, the UV-vis was analyzed to confirm the oxygen vacancy sites on the TS-1 surface. The energy gap profiles were analyzed by TUAC relation as shown in Figure 42(b) because O_V forming affected the lower energy gap (E_g) [65]. The reduction in energy gap might cause surface characteristic changing from semiconductor-like to a more metallic-like. The oxygen atoms were lost until it formed the oxygen vacancy site. So, the lower (E_g) affects the activity of these surfaces. Figure 40(b) revealed that the E_g decreased from 3.00 to 2.70 eV due to the catalyst deactivation after they underwent the MO epoxidation. However, the calcination could enhance the E_g from 2.70 to 2.78 eV which corresponded with the O_V results because the oxygen molecules were added on the TS-1 surface by calcination at 550 °C. Certainly, the TS-1 surface have the oxygen vacancies (O_V) as the deactivation defect which cannot remove by calcination. Its cause that the MO conversion cannot return back to the conversion of fresh catalyst, although the fouling effect is eliminated completely.

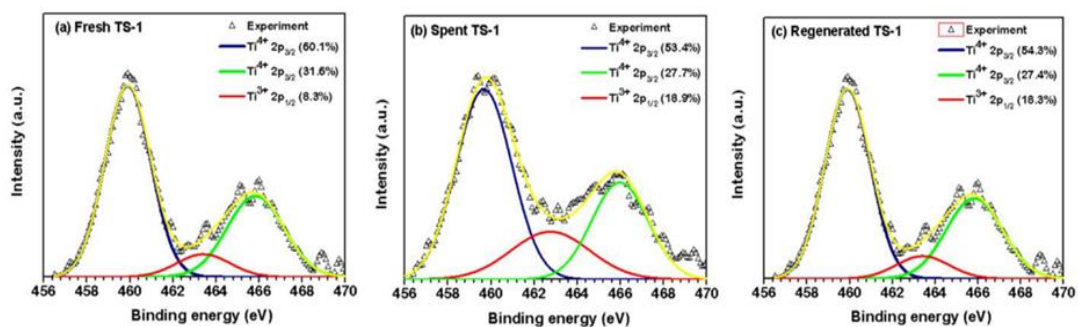


Figure 39 Ti_{2p} XPS spectra of (a) fresh TS-1, (b) spent TS-1, and (c) regenerated TS-1

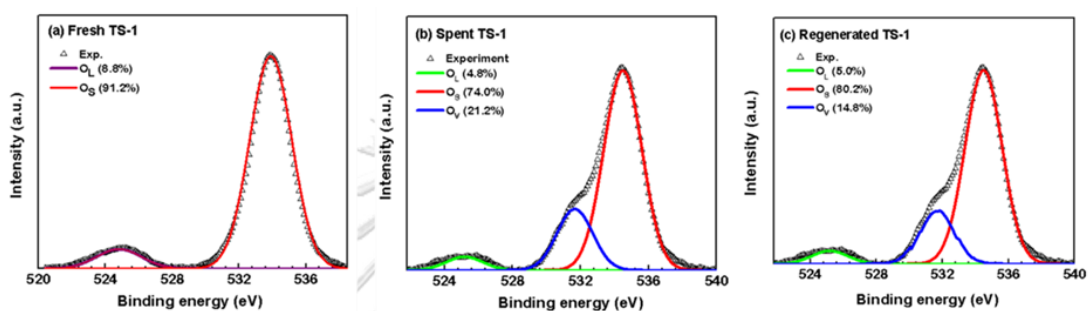


Figure 40. O_{1s} XPS spectra of (a) fresh TS-1, (b) spent TS-1, and (c) regenerated TS-1

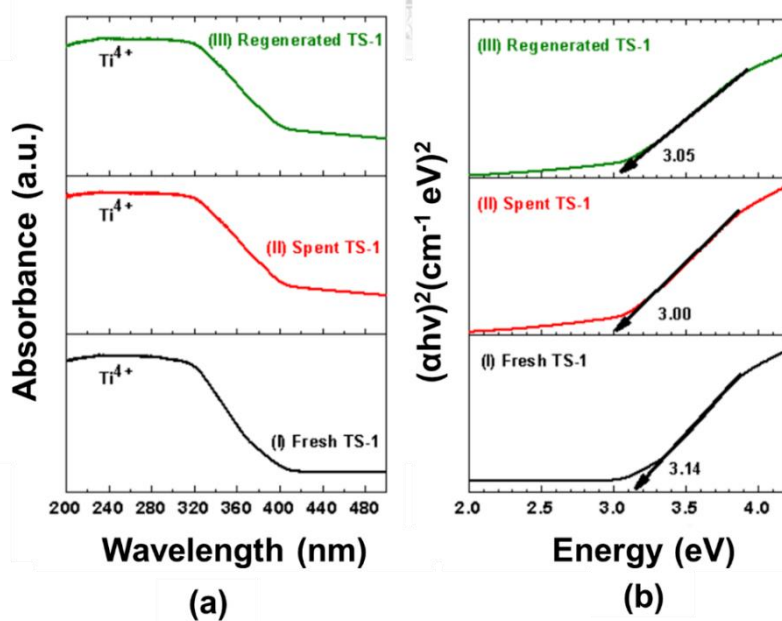


Figure 41. (a) UV spectroscopy profile of (I) fresh TS-1, (II) spent TS-1, and (III) regenerated TS-1 catalysts (b) TUAC relation plot of (I) fresh TS-1, (II) spent TS-1, and (III) regenerated TS-1 catalysts

Table 16 XPS data of different oxidation state of Ti and O on the surface of fresh, spent, and regenerated titanosilicate (TS-1) where O_L represents the lattice oxygen, O_S represents the sub oxide, and O_V represents the oxygen vacancies.

State		Fresh TS-1	Spent TS-1	Regenerated TS-1
Ti ⁴⁺ (unit area)	Ti2p 3/2	3,557.4	3,163.2	3,245.8
	Ti2p 1/2	-	-	-
Total percentage of Ti ⁴⁺		91.7	81.1	81.7
Ti ³⁺ (unit area)	Ti2p 3/2	-	-	-
	Ti2p 1/2	321.6	1,210.0	727.0
Total percentage of Ti ³⁺		8.3	18.9	18.3
O (unit area)	O_L	5,397.5	1,140.0	1,139.3
	O_S	55,759.8	17,755.0	18,251.4
	O_V	-	5,093.9	3,372.3
Total percentage of O_V		-	21.2	14.8

CHAPTER V

CONCLUSIONS AND RECOMMENDATIONS

5.1. Conclusions

The deactivation scheme and surface on P25, TS-1 as the Ti-based catalysts, and $\gamma\text{-Al}_2\text{O}_3$ as the Al-based catalyst probed by the experiments. The results show that the $\gamma\text{-Al}_2\text{O}_3$ yields the highest lower MO conversion as 33.9 followed by TS-1 (18.1) and P25 (17.6), respectively. Besides, the deactivation on P25, TS-1, and $\gamma\text{-Al}_2\text{O}_3$ is found that there are 2 main deactivation effects as: (1) the fouling deposits as the main deactivation on the surface catalyst and (2) the loss of active sites as the oxygen vacancy site and the leaching effect.

Firstly, the fouling effects were found by the TPO results. It provides the fouling which comprises three types, where type1 is found in P25 and $\gamma\text{-Al}_2\text{O}_3$, type2 is uncovered in TS-1 and $\gamma\text{-Al}_2\text{O}_3$, and type3 is appeared in $\gamma\text{-Al}_2\text{O}_3$ only. Also, the FT-IR study indicates that the fouling on P25, TS-1, and $\gamma\text{-Al}_2\text{O}_3$ is: (1) alkane (C-H) and alcohol groups (O-H), (2) α,β -unsaturated ketone (C=O) and alkane groups (C-H), and (3) stretching ester (C=O) and alkane groups (C-H), respectively. Consequently, the $\gamma\text{-Al}_2\text{O}_3$ is more deactivated than P25 and TS-1 because the fouling deposits on $\gamma\text{-Al}_2\text{O}_3$ is stronger adsorption than P25 and TS-1 on the surface.

Secondly, the oxygen vacancy sites were found on the catalyst surface after the reaction for Ti-based catalyst. The effects of oxygen vacancy on both Ti-based catalysts are (1) the change of active site's activity and (2) the reduction of energy gap confirmed by UV-vis technique. This means that if one of the active sites on each Ti-based catalyst is to change to the O-vacancy site, such newly formed vacancy site on the P25 would be more active than the one on the TS 1 surface due to higher electron density, where lower energy gap facilitates the reaction. Since the total conversion of a catalyst depends on (1) the activity of each type of active sites and (2) the total number of each active site on the surface and for that after the deactivation, an active site transforms into the O-vacancy site, a more stable surface is the one that forms a

more active O–vacancy site. Additionally, all catalyst have the leaching effect after running the reaction because the epoxidation occurs in the liquid phase.

In addition, the calcination temperature at 700 °C can be improved the 2nd conversion for γ -Al₂O₃ and at 550 °C for only P25 and TS-1 due to eliminating the fouling deposits completely. Although the fouling effect is eliminated after the regeneration, but the oxygen vacancy (O_v) still exist. Consequently, the O_v sites provide the defects on the surface which the MO conversion cannot return back to the conversion of fresh catalyst.

5.2. Recommendation

- 1) The active site as the hydroperoxo group (X-OOH) cannot characterize directly. It should be selected the more effective way to confirm.
- 2) The oxygen vacancy should be confirmed obviously that cause the loss of the active species to promote the deactivation on the surface.
- 3) The homogeneous catalyst should be studied to solve the selectivity problem from the cracking products.
- 4) The selectivity part should be studied deeply to improve the performance after the regeneration.
- 5) To eliminate the O_v after the reaction, it should be calcined under enriched O₂ to add the oxygen molecules on the surface.
- 6) The another technique for removing the fouling deposits should be studied deeply to regenerate the catalyst such as the solvent extraction.



APPENDIX A

CALCULATION FOR CATALYST PREPARATION

P25 and γ -Al₂O₃ were used the commercial catalyst form AeoXide and Kemaus respectively. For only TS-1 (titanosilicate) was prepared by the hydrothermal method or rapid crystallization. The synthetic gel formed with a molar ratio of 1.0 TiO₂: 7.4 SiO₂: 6.2 (NH₄)₂O: 1.8 TPABr: 553.7 H₂O. Calculation the amount of TIP as the Ti-precursor

1. Calculation the amount of TIP as the Ti-precursor

Based on the amount of TiO ₂	=	0.0055	mol
Molecular weight of TIP	=	284.2	mol/g
Density of TIP	=	0.937	g/mL
So used TIP	=	0.0055 × 284.2	g
	=	1.5631	g
So used TIP solution	=	1.5631 / 0.937	mL
	=	1.6682	mL

2. Calculation the amount of TEOS as the Si-precursor

Based on the amount of SiO ₂	=	0.0055 × 74	mol
	=	0.0407	mol
Molecular weight of TEOS	=	208.3	mol/g
Density of TEOS	=	0.94	g/mL
So used TEOS	=	0.0407 × 208.3	g
	=	8.4778	g
So used TEOS solution	=	8.4778 / 0.94	mL

$$= 9.0189 \quad \text{mL}$$

3. Calculation the amount of NH_4OH solution

$$\text{Based on the amount of } \text{NH}_4\text{OH} = 0.0055 \times 6.2 \quad \text{mol}$$

$$= 0.0341 \quad \text{mol}$$

$$\text{Molecular weight of } \text{NH}_4\text{OH} = 35.0 \quad \text{mol/g}$$

$$\text{Density of } \text{NH}_4\text{OH} = 0.88 \quad \text{g/mL}$$

$$\text{So used } \text{NH}_4\text{OH} = 0.0341 \times 35.0 \quad \text{g}$$

$$= 1.1935 \quad \text{g}$$

$$\text{So used } \text{NH}_4\text{OH solution (28\%)} = 1.1935 / 0.88 \times 100 / 28 \quad \text{mL}$$

$$= 4.8438 \quad \text{mL}$$

4. Calculation the amount of TPABr as the template

$$\text{Based on the amount of TPABr} = 0.0055 \times 1.8 \quad \text{mol}$$

$$= 0.0099 \quad \text{mol}$$

$$\text{Molecular weight of TPABr} = 266.3 \quad \text{mol/g}$$

$$\text{So used TPABr} = 0.0099 \times 266.3 \quad \text{g}$$

$$= 2.6364 \quad \text{g}$$

5. Calculation the amount of DI water

$$\text{Based on the amount of } \text{H}_2\text{O} = 0.0055 \times 553.7 \quad \text{mol}$$

$$= 3.0454 \quad \text{mol}$$

$$\text{Molecular weight of } \text{H}_2\text{O} = 18.0 \quad \text{mol/g}$$

$$\text{Density of } \text{H}_2\text{O} = 1.00 \quad \text{g/mL}$$

$$\begin{aligned} \text{So used H}_2\text{O} &= 3.0454 \times 18.0 \quad \text{g} \\ &= 54.8163 \quad \text{g} \\ \text{So used H}_2\text{O} &= 54.8163 \times 1.00 \quad \text{mL} \\ &= 54.8163 \quad \text{mL} \end{aligned}$$



APPENDIX B

CHARACTERIZATION

This research used many analytical chemistry method to analyze the fresh, spent, and regenerated catalyst as XRD, XPS, UV-vis, TPO, FTIR, and ICP-EOS techniques. This appendix describes the calculation method of some parameter to confirm and discuss the experiment results as follows:

1. Calculation the crystallite size and crystallinity of catalyst by XRD

The crystallite size and crystallinity of catalysts can be calculated by Debye-Scherrer equation (B.1 and B.2) form 2θ profile analysis and FWHM.

$$D = \frac{K\lambda}{\beta \cos \theta} \quad (\text{B.1})$$

Where

D = Average crystallite size of the crystal (nm)

K = Dimensionless shape factor (0.9)

λ = XRD wavelength source (1.5406 nm for Cu-K α)

β = FWHM (radians)

θ = Observed peak position angle (degree)

$$\text{Crystallinity} = \frac{\text{Area of crystal sites}}{\text{Total area}} \times 100 \quad (\text{B.2})$$

Example: Calculation of crystallite size of fresh P25 (TiO₂)

From the XRD patterns of fresh P25, there are many parameters as follows:

Given:

K	=	0.90	
λ	=	1.5406	nm
β	=	0.56808	radians
θ	=	62.7	degree
Crystal area	=	1,288.5816	unit area
Total area	=	1,789.5674	unit area

Solution

D	=	$(0.9 \times 1.5406) / (0.56808 \times \cos(62.7))$	
D	=	20.3269	nm
Crystallinity	=	$(1,288.5816 / 1,789.5674) \times 100$	
	=	71.64489	%

2. Calculation the energy gap of catalysts by UV-vis spectra

The energy gap of catalysts can be calculated by TUAC relation (B.3 and B.4) which it is plotted between $(\alpha h\nu)^2$ (cm⁻¹ eV)² and $h\nu$ (energy, eV) as follows:

$$E = h\nu = \frac{1240}{\lambda \text{ (nm)}} \quad (\text{B.3})$$

Where

E = Energy (eV)

h = Plank constant, 6.625×10^{-34} (J s)

v = Electromagnetic frequencies (s⁻¹)

λ = Wavelength (nm)

$$\alpha = \frac{\text{Thickness}}{\text{Absorbance}} \quad (\text{B.4})$$

Where

α = Absorption coefficient

3. Calculation the percentage of Ti^{4+} , Ti^{3+} , O_L , O_S , and O_V by XPS spectra

The percentage of Ti^{4+} , Ti^{3+} , O_L , O_S , and O_V can be calculated by equation B.5 to observe the Ti and O states before and after the MO epoxidation.

$$\text{The percentage of X} = \frac{\text{Area of X state peak}}{\text{Total area}} \times 100 \quad (\text{B.5})$$

Where

X = Ti^{4+} , Ti^{3+} , O_L , O_S , and O_V state

Example: Calculation of The percentage of O_V of spent P25 catalyst

From the XPS spectra of fresh P25, there are many parameters as follows:

Given:	O_L area	=	4,770.2	unit area
	O_S area	=	7,719.4	unit area
	O_V area	=	3,239.2	unit area

Solution	Total area	=	4,770.2 + 7,719.4 + 3,239.2	
		=	15,728.8	unit area
	% O_V	=	3,239.2 × 100 / 15,728.8	
		=	20.6 %	

REFERENCES



จุฬาลงกรณ์มหาวิทยาลัย
CHULALONGKORN UNIVERSITY

1. Knothe, G., R.O. Dunn, and M.O. Bagby, *Biodiesel: The Use of Vegetable Oils and Their Derivatives as Alternative Diesel Fuels*, in *Fuels and Chemicals from Biomass*. 1997. p. 172-208.
2. Khoobakht, G., et al., *Experimental exergy analysis of transesterification in biodiesel production*. *Energy*, 2020. **196**.
3. Ramos, M.J., et al., *Influence of fatty acid composition of raw materials on biodiesel properties*. *Bioresour Technol*, 2009. **100**(1): p. 261-8.
4. Song, C., et al., *Determination and quantification of fatty acid C=C isomers by epoxidation reaction and liquid chromatography-mass spectrometry*. *Anal Chim Acta*, 2019. **1086**: p. 82-89.
5. Fogassy, G., et al., *Catalyzed ring opening of epoxides: Application to bioplasticizers synthesis*. *Applied Catalysis A: General*, 2011. **393**(1-2): p. 1-8.
6. Wei, Y., et al., *Green and efficient epoxidation of methyl oleate over hierarchical TS-1*. *Chinese Journal of Catalysis*, 2018. **39**(5): p. 964-972.
7. Yunus, R. and X. Luo, *Thermochemical Conversion of Plant Oils and Derivatives to Lubricants*. 2017. p. 183-231.
8. Luo, K., et al., *Visible-light-induced aerobic epoxidation in cyclic ether: Synthesis of spiroepoxyoxindole derivatives*. *Tetrahedron Letters*, 2020. **61**(10).
9. Kamegawa, T., et al., *Synthesis and unique catalytic performance of single-site Ti-containing hierarchical macroporous silica with mesoporous frameworks*. *Langmuir*, 2011. **27**(6): p. 2873-9.
10. Rios, L.A., D.A. Echeverri, and A. Franco, *Epoxidation of jatropha oil using heterogeneous catalysts suitable for the Prileschajew reaction: Acidic resins and immobilized lipase*. *Applied Catalysis A: General*, 2011. **394**(1-2): p. 132-137.
11. Wilde, N., et al., *Epoxidation of biodiesel with hydrogen peroxide over Ti-containing silicate catalysts*. *Microporous and Mesoporous Materials*, 2012. **164**: p. 182-189.
12. Cozzolino, M., et al., *Grafting of titanium alkoxides on high-surface SiO₂ support: An advanced technique for the preparation of nanostructured TiO₂/SiO₂ catalysts*. *Applied Catalysis A: General*, 2007. **325**(2): p. 256-262.

13. Smeets, V., et al., *Mesoporous SiO₂-TiO₂ epoxidation catalysts: Tuning surface polarity to improve performance in the presence of water*. *Molecular Catalysis*, 2018. **452**: p. 123-128.
14. Turco, R., et al., *New findings on soybean and methylester epoxidation with alumina as the catalyst*. *RSC Advances*, 2016. **6**(38): p. 31647-31652.
15. <perrys-chemical-engineering-handbook1.pdf>.
16. Borugadda, V.B. and V.V. Goud, *Epoxidation of Castor Oil Fatty Acid Methyl Esters (COFAME) as a Lubricant base Stock Using Heterogeneous Ion-exchange Resin (IR-120) as a Catalyst*. *Energy Procedia*, 2014. **54**: p. 75-84.
17. Fraile, J.M., et al., *Scope and limitations of one-pot multistep reactions with heterogeneous catalysts: The case of alkene epoxidation coupled to epoxide ring-opening*. *Catalysis Today*, 2011. **173**(1): p. 15-20.
18. Wu, G., et al., *Epoxidation of propylene with H₂O₂ catalyzed by supported TS-1 catalyst in a fixed-bed reactor: Experiments and kinetics*. *Chemical Engineering Journal*, 2013. **215-216**: p. 306-314.
19. Yao, M.-Y., et al., *Highly Efficient Silica-Supported Peroxycarboxylic Acid for the Epoxidation of Unsaturated Fatty Acid Methyl Esters and Vegetable Oils*. *ACS Sustainable Chemistry & Engineering*, 2016. **4**(7): p. 3840-3849.
20. Kholdeeva, O.A., et al., *H₂O₂-based selective epoxidations: Nb-silicates versus Ti-silicates*. *Catalysis Today*, 2019. **333**: p. 63-70.
21. WANG Guangjian, L.Z., LIU Yiwu, LIU Guangqing, XU Mingxia, WANG Lei, *Epoxidation of Styrene with Hydrogen Peroxide over Mn-Ti-Al-MCM-41 Molecular Sieve under Microwave Irradiation*. *CHINESE JOURNAL OF CATALYSIS* 2008. **29**(11): p. 1159–1164.
22. Ramachandran, C.E., et al., *Is 1-hexene epoxidation in TS-1 diffusion limited in different solvents?* *Catalysis Communications*, 2006. **7**(12): p. 936-940.
23. Romero, M.D., et al., *Epoxidation of cyclohexene over basic mixed oxides derived from hydrotalcite materials: Activating agent, solvent and catalyst reutilization*. *Microporous and Mesoporous Materials*, 2008. **111**(1-3): p. 243-253.

24. Drašinac Pajić, N., et al., *Structural stabilization and characterization of active peroxy species on TiO₂-nanotube based materials in mild catalytic wet peroxide oxidation process*. Applied Catalysis A: General, 2018. **562**: p. 276-283.
25. Lu, Z., et al., *Structure and reactivity of single site Ti catalysts for propylene epoxidation*. Journal of Catalysis, 2019. **377**: p. 419-428.
26. Wang, J., et al., *Multilayer structured MFI-type titanosilicate: Synthesis and catalytic properties in selective epoxidation of bulky molecules*. Journal of Catalysis, 2012. **288**: p. 16-23.
27. Yuan, C., Z. Huang, and J. Chen, *Basic ionic liquid supported on mesoporous SBA-15: An efficient heterogeneous catalyst for epoxidation of olefins with H₂O₂ as oxidant*. Catalysis Communications, 2012. **24**: p. 56-60.
28. Kalilur Rahiman, A., et al., *Manganese(III) porphyrin-encapsulated Ti,Si-mesoporous molecular sieves as heterogeneous catalysts for the epoxidation of alkenes*. Applied Catalysis A: General, 2006. **314**(2): p. 216-225.
29. Sha, S., et al., *Co(II) coordinated metal-organic framework: An efficient catalyst for heterogeneous aerobic olefins epoxidation*. Catalysis Communications, 2014. **43**: p. 146-150.
30. Ma, X.T., et al., *Catalytic epoxidation of cyclic alkenes with air over CoO_x/zeolite heterogeneous catalysts*. Catalysis Communications, 2015. **67**: p. 98-102.
31. Lignier, P., et al., *Effect of the titania morphology on the Au/TiO₂-catalyzed aerobic epoxidation of stilbene*. Catalysis Today, 2009. **141**(3-4): p. 355-360.
32. Pescarmona, P. and P. Jacobs, *A high-throughput experimentation study of the epoxidation of alkenes with transition-metal-free heterogeneous catalysts*. Catalysis Today, 2008. **137**(1): p. 52-60.
33. Michiel C. A. van Vliet, I.W.C.E.a.R.A.S., *Methyltrioxorhenium-catalysed epoxidation of alkenes in trifluoroethanol*. 1999.
34. Zhang, Y., et al., *Palladium nanoparticles supported on UiO-66-NH₂ as heterogeneous catalyst for epoxidation of styrene*. Inorganic Chemistry Communications, 2019. **100**: p. 51-55.

35. Shen, Y., et al., *Highly selective mono-epoxidation of dicyclopentadiene with aqueous H_2O_2 over heterogeneous peroxo-phosphotungstic catalysts*. *Molecular Catalysis*, 2017. **433**: p. 185-192.
36. Nishimura, A., et al., *Reforming Characteristics under Visible Light Response of Cr- or Ag-Doped Prepared by Sol-Gel and Dip-Coating Process*. *International Journal of Photoenergy*, 2012. **2012**: p. 1-12.
37. Regonini, D., et al., *A review of growth mechanism, structure and crystallinity of anodized TiO_2 nanotubes*. *Materials Science and Engineering: R: Reports*, 2013. **74**(12): p. 377-406.
38. Yu, L., et al., *Electron transportation path build for superior photoelectrochemical performance of Ag_3PO_4/TiO_2* . *RSC Advances*, 2017. **7**(86): p. 54485-54490.
39. Wu, H., et al., *Effect of TiO_2 calcination temperature on the photocatalytic oxidation of gaseous NH_3* . *Journal of Environmental Sciences*, 2014. **26**(3): p. 673-682.
40. Yang, Y., et al., *Hierarchical Ti-containing hollow-structured zeolite synthesized by seed-assisted method for catalytic epoxidation of alkenes efficiently*. *Materials Chemistry and Physics*, 2019. **236**.
41. Paul F. Henry, M.T.W., and Chick C. Wilson, *Structural Investigation of TS-1: Determination of the True Nonrandom Titanium Framework Substitution and Silicon Vacancy Distribution from Powder Neutron Diffraction Studies Using Isotopes*. 2001.
42. Li, J., et al., *Effect of iron and phosphorus on HZSM-5 in catalytic cracking of 1-butene*. *Fuel Processing Technology*, 2015. **134**: p. 32-38.
43. Ratnasamy, P., D. Srinivas, and H. Knözinger, *Active Sites and Reactive Intermediates in Titanium Silicate Molecular Sieves*. 2004. p. 1-169.
44. Wang, B., et al., *Hierarchical TS-1 synthesized via the dissolution-recrystallization process: Influence of ammonium salts*. *Catalysis Communications*, 2017. **101**: p. 26-30.

45. Wilde, N., et al., *Highly efficient nano-sized TS-1 with micro-/mesoporosity from desilication and recrystallization for the epoxidation of biodiesel with H₂O₂*. *Green Chemistry*, 2015. **17**(6): p. 3378-3389.
46. M.A. Uguina , D.P.S., G. Ovejero, R. Van Grieken, M. Camacho, *Preparation of TS-1 by wetness impregnation of amorphous SiO₂-TiO₂ solids: influence of the synthesis variables*. 1995.
47. Simón Y. Reyes López, J.S.R., Satoshi Sugita Sueyoshi, *Low-Temperature Formation of Alpha Alumina Powders via Metal Organic Synthesis*. 2006.
48. Aboul-Fotouh, S.M.K., *Production of dimethylether (DME) as a clean fuel using sonochemically prepared CuO and/or ZnO-modified γ -alumina catalysts*. *Journal of Fuel Chemistry and Technology*, 2014. **42**(3): p. 350-356.
49. Tjokorde Walmiki Samadhi, S., Kevin R. Lismana & Khasin Fuadi, *Synthesis of gamma Al₂O₃ Catalyst Support from Kaolin of Indonesian Origin*. 2011.
50. Xie, Y., et al., *The Effect of Novel Synthetic Methods and Parameters Control on Morphology of Nano-alumina Particles*. *Nanoscale Res Lett*, 2016. **11**(1): p. 259.
51. Lu, X., X. Cui, and M. Song, *Study on the alteration of chemical composition and structural parameters of modified montmorillonite*. *Minerals Engineering*, 2003. **16**(11): p. 1303-1306.
52. Akira Takahashi, F.H.Y., and Ralph T. Yang, *New Sorbents for Desulfurization by δ -Complexation: Thiophene/ Benzene Adsorption*. 2002.
53. Lu, X., et al., *Effects of phase transformation on properties of alumina ceramic membrane: A new assessment based on quantitative X-ray diffraction (QXRD)*. *Chemical Engineering Science*, 2019. **199**: p. 349-358.
54. Rinaldi, R., J. Sepúlveda, and U. Schuchardt, *Cyclohexene and Cyclooctene Epoxidation with Aqueous Hydrogen Peroxide using Transition Metal-Free Sol-Gel Alumina as Catalyst*. *Advanced Synthesis & Catalysis*, 2004. **346**(23): p. 281-285.
55. Choudhary, V.R., et al., *Epoxidation of styrene by anhydrous hydrogen peroxide over boehmite and alumina catalysts with continuous removal of the reaction water*. *Journal of Molecular Catalysis A: Chemical*, 2005. **227**(1-2): p. 217-222.

56. Bharti, B., et al., *Formation of oxygen vacancies and Ti(3+) state in TiO₂ thin film and enhanced optical properties by air plasma treatment*. Sci Rep, 2016. **6**: p. 32355.
57. Zhang, Y.S., et al., *A study of coke formed by heavy oil volatilization/decomposition on Y-zeolite*. Journal of Analytical and Applied Pyrolysis, 2019. **141**.
58. Hayashi, K., et al., *Isolation, characterization, and reactivity of the reaction products of the dimeric, Ti–O–Ti bridged anhydride form of the 1,2-dititanium(IV)-substituted α -Keggin polyoxometalate with aqueous 30% H₂O₂*. Journal of Molecular Catalysis A: Chemical, 2007. **262**(1-2): p. 30-35.
59. Janković, B., et al., *The assessment of spontaneous ignition potential of coals using TGA–DTG technique*. Combustion and Flame, 2020. **211**: p. 32-43.
60. Gou, M.-L., et al., *Coking and deactivation behavior of ZSM-5 during the isomerization of styrene oxide to phenylacetaldehyde*. Catalysis Communications, 2017. **98**: p. 116-120.
61. Kurańska, M., et al., *Effect of homogeneous catalysts on ring opening reactions of epoxidized cooking oils*. Journal of Cleaner Production, 2019. **230**: p. 162-169.
62. Cordero-Lanzac, T., et al., *Characterization and controlled combustion of carbonaceous deactivating species deposited on an activated carbon-based catalyst*. Chemical Engineering Journal, 2017. **327**: p. 454-464.
63. Marafi, A., A. Hauser, and A. Stanislaus, *Deactivation patterns of Mo/Al₂O₃, Ni–Mo/Al₂O₃ and Ni–MoP/Al₂O₃ catalysts in atmospheric residue hydrodesulphurization*. Catalysis Today, 2007. **125**(3-4): p. 192-202.
64. Sanjinés, R., et al., *Electronic structure of anatase TiO₂oxide*. Journal of Applied Physics, 1994. **75**(6): p. 2945-2951.
65. Gerosa, M., et al., *Defect calculations in semiconductors through a dielectric-dependent hybrid DFT functional: The case of oxygen vacancies in metal oxides*. J Chem Phys, 2015. **143**(13): p. 134702.

66. Liu, C., et al., *Ti leaching differences during acid leaching of coal gangue based on different thermal fields*. *Waste Manag*, 2020. **101**: p. 66-73



VITA

NAME Kanokpon Maungthong

DATE OF BIRTH 11 September 1995

PLACE OF BIRTH Bangkok, Thailand

INSTITUTIONS ATTENDED 2014 - Graduated high school from Watrajabophit School.
2018 - Graduated Bachelor's Degrees from Faculty of Engineering in Chemical Engineering, King Mongkut's Institute of Technology Ladkrabang, Bangkok, Thailand.

HOME ADDRESS 387 Isaraphap 5 Alley, Somdet Chao Phraya Sub-district, Khlong San, Bangkok 10600, Thailand



จุฬาลงกรณ์มหาวิทยาลัย
CHULALONGKORN UNIVERSITY